2015

Joint leaf chlorophyll content and leaf area index retrieval from Landsat data using a regularized model inversion system (REGFLEC)

Rasmus Houborg
King Abdullah University of Science and Technology, rasmus.houborg@kaust.edu.sa

Matthew McCabe
King Abdullah University of Science and Technology, matthew.mccabe@kaust.edu.sa

Alessandro Cescatti
Institute for Environment and Sustainability

Feng Gao
USDA-ARS Hydrology and Remote Sensing Laboratory, Feng.Gao@ars.usda.gov

Mitchell Schull
USDA-ARS Hydrology and Remote Sensing Laboratory

See next page for additional authors

Authors

Rasmus Houborg, Matthew McCabe, Alessandro Cescatti, Feng Gao, Mitchell Schull, and Anatoly A. Gitelson

CrossMark

Joint leaf chlorophyll content and leaf area index retrieval from Landsat data using a regularized model inversion system (REGFLEC)

Rasmus Houborg [a,*], Matthew McCabe [a], Alessandro Cescatti [b], Feng Gao [c], Mitchell Schull [c], Anatoly Gitelson [d]

[a] King Abdullah University of Science and Technology, Water Desalination and Reuse Center, Kingdom of Saudi Arabia
[b] European Commission, Joint Research Centre, Institute for Environment and Sustainability, Ispra, Italy
[c] USDA-ARS Hydrology and Remote Sensing Laboratory, Beltsville, MD, USA
[d] Center for Advanced Land Management Information Technology (CALMIT), School of Natural Resources, University of Nebraska-Lincoln, Lincoln, NE, USA

ABSTRACT

Leaf area index (LAI) and leaf chlorophyll content (Chl_l) represent key biophysical and biochemical controls on water, energy and carbon exchange processes in the terrestrial biosphere. In combination, LAI and Chl_l provide critical information on vegetation density, vitality and photosynthetic potentials. However, simultaneous retrieval of LAI and Chl_l from space observations is extremely challenging. Regularization strategies are required to increase the robustness and accuracy of retrieved properties and enable more reliable separation of soil, leaf and canopy parameters. To address these challenges, the REGularized canopy reFLECtance model (REGFLEC) inversion system was refined to incorporate enhanced techniques for exploiting ancillary LAI and temporal information derived from multiple satellite scenes. In this current analysis, REGFLEC is applied to a time-series of Landsat data.

A novel aspect of the REGFLEC approach is the fact that no site-specific data are required to calibrate the model, which may be run in a largely automated fashion using information extracted entirely from image-based and other widely available datasets. Validation results, based upon in-situ LAI and Chl_l observations collected over maize and soybean fields in central Nebraska for the period 2001–2005, demonstrate Chl_l retrieval with a relative root-mean-square-deviation (RMSD) on the order of 19% (RMSD = 8.42 μg cm^{-2}). While Chl_l retrievals were clearly influenced by the version of the leaf optical properties model used (PROSPECT), the application of spatio-temporal regularization constraints was shown to be critical for estimating Chl_l with sufficient accuracy. REGFLEC also reproduced the dynamics of in-situ measured LAI well ($r^2 = 0.85$), but estimates were biased low, particularly over maize (LAI was underestimated by ~36 %). This disparity may be attributed to differences between effective and true LAI caused by significant foliage clumping not being properly accounted for in the canopy reflectance model (SAIL). Additional advances in the retrieval of canopy biophysical and leaf biochemical constituents will require innovative use of existing remote sensing data within physically realistic canopy reflectance models along with the ability to exploit the enhanced spectral and spatial capabilities of upcoming satellite systems.

© 2014 Elsevier Inc. All rights reserved.

1. Introduction

The ability to accurately model fluxes of carbon dioxide, water vapor and heat in the terrestrial biosphere is important for improving water resource management, agricultural productivity and our understanding of ecosystem functioning. However, the capacity to do this depends on 1) the physical realism of the model employed (Kalma, McVicar & McCabe, 2008), 2) the quality of meteorological model forcing fields (Ershadi, McCabe, Evans, Mariethoz & Kavetski, 2013) and 3) the ability to specify model inputs and parameters with adequate accuracy (Jung

et al., 2007; Zaehle, 2005). State of the art process-oriented terrestrial biosphere models (TBMs) may be characterized by improved process understanding, but many of the parameters controlling vegetation structure and function can be challenging to define with acceptable accuracy over spatial and temporal domains (Groenendijk et al., 2011; Knorr & Heimann, 2001; Wang, Baldocchi, Leuning, Falge & Vesala, 2007). Remote sensing can support such modeling efforts by offering spatially and temporally distributed information on important vegetation characteristics, which would be very difficult to obtain otherwise. Likewise, the integration of observation based model constraints (Dorigo et al., 2007; Houborg, Cescatti, Migliavacca & Kustas, 2013; Kaminski et al., 2012) are key towards reducing uncertainties of model predicted surface fluxes in space and time (Bonan et al., 2011; McCabe, Kalma & Franks, 2005). To advance these issues, the work presented here focuses on the retrieval of canopy biophysical and leaf

biochemical constituents and their use as potential constraints in spatially and temporally distributed model simulations.

Leaf Area Index (LAI), defined as one-sided green leaf area per unit of horizontal ground area, is a key biophysical parameter used in most TBMs that often functions as the primary remote sensing based descriptor of vegetation density, phenology and distribution across a landscape (Bonan et al., 2011; Medvigy, Wofsy, Munger, Hollinger & Moorcroft, 2009; Sellers et al., 1996). Mapping LAI using remotely sensed data has been a major community objective (e.g. Bacour, Baret, Béal, Weiss & Pavageau, 2006; Chen & Cihlar, 1996; Gray & Song, 2012; Knyazikhin, Martonchik, Myneni, Diner & Running, 1998; Viña, Gitelson, Nguy-Robertson & Peng, 2011) and a range of multi-year validated global and regional datasets of LAI have been made available at resolutions of ~1 km based on medium resolution optical sensors such as MODIS (Myneni et al., 2002; Yang et al., 2006), SPOT/VEGETATION (Baret et al., 2007, 2013) and MODIS/MISR (Pinty et al., 2011). Reported accuracies (direct validation against in-situ measurements) vary widely, but typically range between 0.5 and 1.0 LAI units root-mean-square-difference (RMSD) (Garrigues et al., 2008; Yang et al., 2006; http://landval.gsfc.nasa.gov/), although significantly higher errors may occur as a result of land cover misclassification and large uncertainties in surface reflectance due to aerosol and cloud contamination. Finer spatial resolution LAI is required to effectively resolve processes in heterogeneous landscapes at the scale of individual fields, and recent studies have investigated the prospect of generating potentially global LAI from Landsat surface reflectance data. These include a physically-based algorithm that uses canopy spectral invariants theory (Ganguly et al., 2012), as well as a reference-based methodology that uses high-quality LAI retrievals from MODIS to produce MODIS consistent Landsat-resolution LAI (Gao, Anderson, Kustas & Wang, 2012). For the latter a mean absolute difference of 0.23 was reported based on a comparison against measurements aggregated to the field scale (Gao, Anderson, Kustas & Wang, 2012).

While accurate LAI inputs are essential for modeling land surface processes at different spatial scales, there is a need to implement supplemental remote sensing based determinants of vegetation function in order to better diagnose spatiotemporal variations in overall plant physiological condition and photosynthetic performance. Leaf chlorophyll content (Chl$_l$), defined as total chlorophyll content [chlorophyll a + chlorophyll b] on a leaf area basis, may serve as an additional and potentially important variable for land-surface remote sensing because of its close relationship to leaf nitrogen (Evans, 1989; Sage, Pearcy & Seeman, 1987) and thus leaf photosynthetic capacity (Houborg, Cescatti, Migliavacca & Kustas, 2013; Kattge, Knorr, Raddatz & Wirth, 2009). Chl$_l$ level differs according to plant species and for a given plant type there may be a significant evolution of Chl content along the leaf cycle, as modulated by changes in nutrient and water availability, environmental conditions and plant phenology (Evans, 1989; Schlemmer et al., 2013; Xu & Baldocchi, 2003). The use of Chl$_l$ as a proxy for plant physiological status and photosynthetic functioning is convenient in a remote sensing context as it directly controls leaf absorption in the visible region. Chl$_l$ may be retrieved from satellite observed reflectances by inversion of leaf optics and canopy reflectance models (Jacquemoud et al., 2009). However, retrieving Chl$_l$ from space observations is challenging as the influence of atmospheric effects, canopy characteristics and background reflectance may confound the detection of relatively subtle differences in canopy reflectance resulting from changes in Chl$_l$ (Daughtry, Walthall, Kim & Colstoun, 2000). Accordingly, remote estimation of Chl$_l$ has been associated with fairly large uncertainties, with reported accuracies typically ranging between 8 and 15 µg cm^{-2} RMSD based on a variety of empirical and physically-based approaches and sensor data (e.g. Bacour et al., 2002; Botha, Leblon, Zebarth & Watmough, 2007; Delegido, Vergara, Verrelst, Gandía & Moreno, 2011; Houborg & Anderson, 2009; Jacquemoud, Baret, Andrieu, Danson & Jaggard, 1995). The chlorophyll predictive ability of the PROSPECT leaf optical properties model, that form the

basis of most radiative transfer model inversion studies (Jacquemoud et al., 2009), is in itself on the order of 9–10 µg cm^{-2} RMSD (Feret et al., 2008, 2011).

In physically based frameworks, the accuracy of LAI and Chl$_l$ estimates depend in part on the ability to regularize the ill-posed inverse problem caused by measurement and model uncertainties and the limited information carried by the radiometric signal. Indeed, different combinations of model parameters can produce almost identical spectra (Baret & Buis, 2008; Combal, Baret, Weiss & Trubuil, 2002; Weiss, Baret, Myneni, Pragnère & Knyazikhin, 2000), resulting in non-unique solutions. Regularization strategies are required to increase the robustness and accuracy of retrieved properties and to improve the separation of soil, leaf and canopy variables. Introducing prior information on the distribution of model variables, canopy characteristics and soil background conditions may significantly improve the estimation accuracy of biophysical variables (Combal, Baret, Weiss & Trubuil, 2002; Darvishzadeh, Skidmore, Schlerf & Atzberger, 2008; Koetz, Baret, Poilvé & Hill, 2005). However, this regularization technique typically relies on the existence of experimental data collected at the site of interest and the calibrated models may have limited applicability over other sites and land cover types.

Ultimately, the goal is to develop versatile and automated image-based methodologies that can be applied over a diversity of land cover types, soil backgrounds and atmospheric conditions, while removing the need for site-specific calibration. To do this, the amount of information used in the inversion process needs to be increased by considering either 1) image-based prior information on land cover and phenological LAI dynamics (Dorigo, Richter, Baret, Bamler & Wagner, 2009; Houborg, Soegaard & Boegh, 2007; Koetz, Baret, Poilvé & Hill, 2005), 2) additional spectral bands with optimized sensitivity to the parameters of interest (Clevers & Gitelson, 2013; Delegido, Alonso, González & Moreno, 2010), 3) multi-angular information (Bacour et al., 2002; Vuolo, Dini & D'Urso, 2008), 4) the addition of noise and multiple solutions in the inversion (Rivera, Verrelst, Leonenko & Moreno, 2013) or 4) spatial and temporal constraints such as spectral signatures of adjacent pixels (Atzberger, 2004; Atzberger & Richter, 2012) and multi-temporal-patch inversion (Lauvernet, Baret, Hascoët, Buis & Le Dimet, 2008).

The regularized canopy reflectance model (REGFLEC) couples leaf, canopy and atmospheric radiative transfer models and utilizes a multi-step regularized inversion approach for retrieving LAI and Chl$_l$ from multi-spectral at-sensor radiance data (Houborg & Anderson, 2009). REGFLEC introduces various image-based constraints in an effort to solve the inverse problem, such as separate retrieval of soil background reflectance and leaf/canopy characteristics, use of ancillary image-based information, and utilization of the radiometric information of associated pixels for estimating an optimal set of class-invariant vegetation parameters (Houborg & Anderson, 2009; Houborg, Cescatti, Migliavacca & Kustas, 2013). The model then establishes a suite of predictive vegetation index (VI) relationships, specific to each scene and dependent on land cover class, soil background and atmospheric conditions, in order to map LAI and leaf Chl content over the modeling domain.

The work presented here establishes important refinements to the REGFLEC retrieval system and its application to multi-spectral Landsat satellite time-series data for joint LAI and Chl$_l$ retrieval. A key objective of this study is to demonstrate the achievable accuracy of LAI and Chl$_l$ estimation using a few standard broad spectral bands available operationally (i.e. green, red and near-infrared) and to evaluate the impact of various spatio-temporal constraints and REGFLEC configurations on LAI and Chl$_l$ retrieval accuracies. An extensive dataset of in-situ LAI and Chl$_l$ collected over maize and soybean sites in central Nebraska over a 5-year period (2001–2005) is used for validation. The atmospheric and canopy radiative transfer models that form the basis of REGFLEC are briefly described in Sections 2.1 and 2.2, followed by a detailed description of the REGFLEC retrieval system (Section 2.3). Additional Sections outlining the study area are presented in Section

2.4, along with biophysical field measurements (Section 2.5) and information on the Landsat data and REGFLEC setup process in Section 2.6. Results are presented and discussed in Section 3.

2. Approach and methodology

2.1. Atmospheric radiative transfer model

The vector version of the 6S (Second Simulation of the Satellite Signal in the Solar Spectrum) atmospheric radiative transfer model (Kotchenova, Vermote, Matarrese & Klemm, 2006; Vermote, Tanre, Deuze, Herman & Morcette, 1997) is used for converting at-sensor radiances to directional surface reflectances. As further detailed in Houborg et al. (2009), 6S simulates the reflection of solar radiation by a coupled atmosphere-surface system for a wide range of atmospheric, spectral and geometrical conditions and it has demonstrated good performance (Kotchenova, Vermote, Matarrese & Klemm, 2006; Proud et al., 2010; Vermote, Tanre, Deuze, Herman & Morcette, 1997). Input parameters include surface elevation, sun zenith (θ_{sz}), view zenith (θ_{vz}), sun azimuth (θ_{az}) and satellite azimuth (θ_{saz}) angles, total column ozone (O_3), aerosol optical thickness at 550 nm (τ_{550}), total precipitable water (TPW), and aerosol volume and size distribution.

2.2. Canopy reflectance (CR) model

The Markov chain canopy reflectance model, ACRM (Kuusk, 2001) and the Scattering by Arbitrary Inclined Leaves model, 4SAIL (Verhoef, 1984, 1985; Verhoef, Jia, Xiao & Su, 2007), both with a hot-spot correction implemented (Kuusk, 1991), consider the canopy as a turbid medium in which leaves are randomly distributed in space (canopy is considered horizontally homogeneous). The models operate in the spectral domain 400–2500 nm and calculate directional canopy reflectance at a spectral resolution of 1 nm given the observation geometry, canopy structure, leaf reflectance and transmittance and soil reflectance. This study focuses exclusively on REGFLEC applications based on the 4SAIL model, which is the most widely used CR model in the remote sensing community (Jacquemoud et al., 2009). In 4SAIL, canopy structure is characterized by LAI, leaf angle distribution (LAD), and hot-spot parameter (S_L). In the version used here, LAD is assumed ellipsoidal and represented by the mean leaf inclination angle (θ_l) (Campbell, 1986). Soil spectral reflectance is approximated as a function of two soil parameters (s_1 and s_2) (Houborg & Boegh, 2008; Price, 1990) and a parameter (f_B), representing the canopy fraction of senescent leaf material, is incorporated (Houborg & Anderson, 2009). The model sensitivity to S_L is generally low for near-nadir viewing directions and is parameterized here as a function of LAI (Verhoef & Bach, 2003). The wavelength dependent relative proportion of direct and diffuse flux in incoming radiation is calculated as a function of τ_{550}.

Leaf spectral reflectance and transmittance for green and senescent leaves are simulated using the leaf optical PROperties SPECTra (PROSPECT) model (Feret et al., 2008; Jacquemoud & Baret, 1990). The input variables of PROSPECT are the leaf mesophyll structure parameter (N), which is related to leaf thickness and cellular arrangement, leaf chlorophyll *a* and *b* content (Chl_l), leaf water content (C_w), dry matter content (C_m), and leaf brown pigment (C_{bp}). C_w is not considered here given that leaf water does not affect leaf reflectance in the visible to near-infrared domain. The N, Chl_l and C_m of senescent leaf material is fixed at 3, 5 μg cm^{-2} and 100 g m^{-2}, respectively and green and senescent leaf material is assumed to be completely dissociated (Verhoef & Bach, 2003).

Canopy reflectance spectra representative of intermixed green and senescent leaves are simulated by weighing the leaf reflectance and transmittance spectra for green ($C_{bp} = 0$) and senescent ($C_{bp} = 1$) leaves with f_B (Houborg & Anderson, 2009). In PROSPECT, the specific absorption coefficients and the refractive index of leaf material are determined on the basis of experimental data. Feret et al. (2008)

reassessed the refractive index and absorption coefficients based on a comprehensive dataset of leaf biochemical and optical properties, giving rise to two new versions: PROSPECT-4 (P4) and PROSPECT-5 (P5), with the latter version providing separate treatment of chlorophylls and carotenoids (Fig. 1a). REGFLEC implements both of these as well as the original version (PROSPECT-3; Baret & Fourty, 1997). The three calibrations are characterized by significant differences in the Chl specific absorption coefficients, with P5 and particularly P4 displaying higher contrasts between non-absorption (550 nm) and absorption wavelengths (450 and 680 nm) compared to the flatness of P3 (Fig. 1a). Although P5 is included as an option in REGFLEC, the carotenoids content (Car) is not yet specifically treated and set to zero, assuming that absorption of light by photosynthetic pigments is entirely caused by chlorophylls. In this form, light absorption in P5 is in closer agreement with P3 over the blue to beginning of the green waveband region (400–540 nm) (Fig. 1a). Accordingly, modeled canopy reflectances using P5 and P3 agree closely in the blue band of Landsat 7 (Fig. 1b). In contrast large divergences in simulated canopy reflectances occur in the chlorophyll sensitive green band as a result of using P5, P4 or P3 (Fig. 1b). The effect of the adopted PROSPECT calibration on the LAI and Chl_l retrieval results are evaluated in Section 3.3.1.

2.3. The REGularized canopy reFLECtance model (REGFLEC)

REGFLEC (see www.regflec.com) (Fig. 2) combines the atmospheric radiative transfer (Section 2.1) and canopy reflectance (Section 2.2) models for translating at-sensor radiance observations from a multispectral sensor like Landsat into maps of Chl_l and LAI. REGFLEC adopts a Look-Up-Table (LUT) based inversion scheme and implements spatial and temporal regularization strategies in an effort to better control the confounding influence of atmospheric effects, leaf and canopy characteristics and soil background on retrieved biophysical properties, based entirely on image-based methodologies.

As shown in Fig. 2, the REGFLEC (Version 2.5) retrieval approach consists of 7 steps, including largely automated routines for (1) multi-scene resizing, co-registration and cloud screening (Section A.1), (2) atmospheric correction (Section A.1), (3) land cover classification (Section A.2), (4) forward runs with the CR model for computing LUTs of spectral reflectances and VIs (Section A.3), (5) initial estimation of the soil background signal (Section A.4), (6) retrieval of optimal class-invariant vegetation parameters (Section A.5), and (7) pixel-wise mapping of LAI and Chl_l based on a suite of appropriate spectral reflectance relationships (Section A.6). Retrieved values are informed by preceding steps to reflect pixel-specific differences in view and illumination geometry, land cover class, phenological stage, soil background and atmospheric condition. In step 6, multi-scene spectral reflectance observations over dense vegetated pixels are exploited to constrain the retrieval of the class-specific parameters. The inversion process may also make use of ancillary LAI, derived independently from satellite data (Section A.7), as an additional constraint in an effort to improve the separation of LAI and Chl_l effects on observed reflectance spectra. The REGFLEC multi-step retrieval and regularization methodology is described in greater detail in Appendix A.

The overall idea of LUT approaches is to find the model parameter combination that yield the best fit between measured and modeled LUT spectra, which is typically achieved by minimizing a merit function based on the RMSD or mean absolute error (MAE). In REGFLEC, the optimal parameter combination (i.e. LAI, Chl_l, N, θ_l, f_B, C_m, s_1, and s_2) is not determined in a single LUT inversion. Instead, soil parameters and class-specific vegetation parameters are retrieved separately (step 5 and 6) before mapping LAI and Chl_l over the modeling domain (step 7). Optimal solutions are achieved by minimizing the MAE between modeled and measured reflectances and assigning penalties (e.g. for out of range conditions) as detailed in Houborg and Anderson (2009). In addition, the LUT inversion is iterative in that the minimization function is evaluated for a range of plausible parameter combinations, by using the LUTs
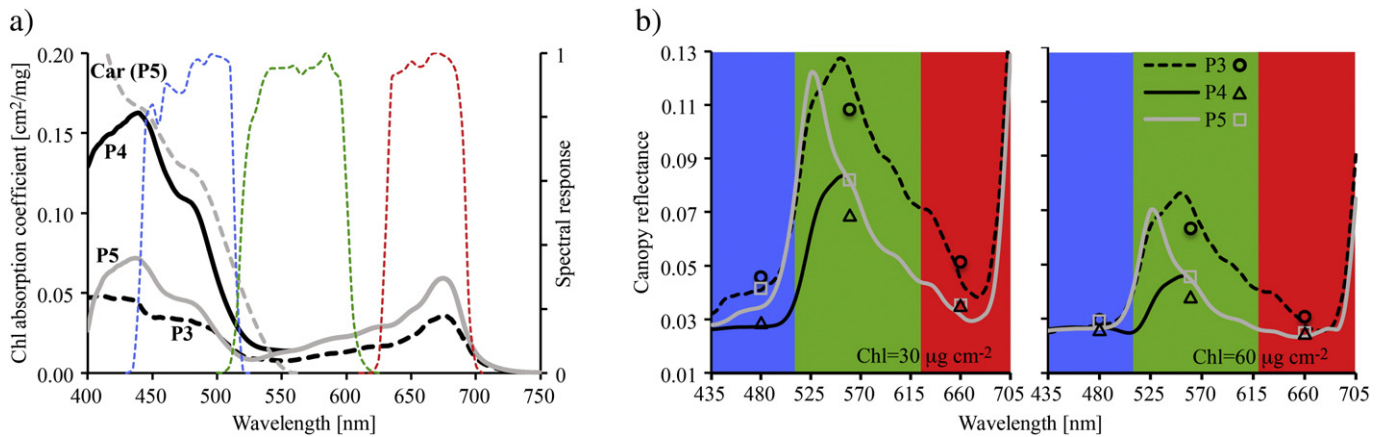
Fig. 1. a) Spectral variability of the Chlorophyll *a* and *b* specific absorption coefficients used in PROSPECT-5 (P5), PROSPECT-4 (P4), and PROSPECT-3 (P3). For P5, the specific absorption coefficients of the carotenoid content (Car) are also shown, although this component is not specifically treated (Car = 0) in the current REGFLEC implementation of P5. Spectral response filters of the Landsat-7 blue, green and red bands are shown using the secondary y-axis. b) SAIL-PROSPECT simulated canopy reflectances using the three PROSPECT versions for two different values of Chl (30 and 60 μg cm^{-2}). The symbols represent integrated reflectance values over the blue, green and red wavelength region using the Landsat-7 response filters (a). For these simulations, LAI = 4, θ_l = 55, s_1 = 0.2, N = 1.8, C_m = 30, f_B = 0, θ_s = 30, θ_v = 0.

in both forward and inverse mode for calculating LAI/Chl_l and reflectances, as described further in Section A.3 to A.5. The advantage of this alternative iterative LUT approach is that it is more flexible, less sensitive to LUT parameter entry values (Section A.3) and facilitates integration of spatial and temporal constraints such as the ancillary LAI and multi-scene constraint.

REGFLEC is planned to be made available for distribution primarily to researchers interested in refining and further developing certain aspects of the retrieval system. An online submission system is being developed to facilitate streamlined web-based processing requests for regions and time-periods of interest. The REGFLEC job requests will be queued on a central in-house processing unit, automatically executed and providing time-series imagery distributed via FTP.

2.4. Study area

LAI and Chl_l measurements from three sites (Ne1, Ne2, Ne3) located at the University of Nebraska-Lincoln Agricultural Research and Development Center near Mead, Nebraska (http://ameriflux.ornl.gov/fullsiteinfo.php?sid=72) (Fig. 3), were used for validating REGFLEC retrievals. The three sites are all approximately 65-ha fields located within 1.6 km of each other. Ne1 has been continuously under maize since 2001, whereas Ne2 and Ne3 are under a maize-soybean rotation. Ne1 and Ne2 are both irrigated with a center pivot system, whereas Ne3 is rainfed. The region is characterized by a temperate continental climate with the growing season beginning in May and ending in October. Maize is characterized by a longer growing season than soybean and period of peak green-up typically precedes soybean by approximately 2–3 weeks. This study focuses on data collected over a five-year period (2001–2005) covering all phenological stages found in maize and soybean (Gitelson et al., 2012). The annual precipitation totals ranged from 475 mm (2001) to 670 mm (2004), and the precipitation totals for the months of July and August were lowest in 2001 (96 mm) and 2003 (70 mm) (compared to 219 mm, 114 mm, and 142 mm in 2002, 2004 and 2005, respectively), resulting in water limited crop conditions at the rainfed Ne3 site (Verma et al., 2005). Irrigation at Ne1 and Ne2 approximately doubles the amount of water available when compared to precipitation alone (Kalfas, Xiao, Vanegas, Verma & Suyker, 2011). A detailed description of the sites is given in (Verma et al., 2005).

2.5. Field measurements of LAI and Chl_l

Within each of the three fields, six small (20x20 m) intensive measurements zones (IMZ) have been carefully established to represent

the spatial variability in soil type, landscape features, and crop production potential as a basis for accurate upscaling of ground measurements to the whole-field level (Verma et al., 2005). Green LAI was determined from destructive samples in each IMZ at approximately 10 to 14 day intervals and data at the six IMZs were area-weighted averaged to obtain field-wide representative values (Gitelson, Vina, et al., 2003). Fraction of green leaves (fg) was derived from the destructive measurements of green and total LAI. Chl_l was estimated non-destructively using reflectance measurements of upper canopy leaves collected in-situ on maize and soybean leaves using a spectroradiometer equipped with a leaf clip as described in (Gitelson, Vina, Ciganda, Rundquist & Arkebauer, 2005). Chl_l determined analytically in the lab was related to the red edge chlorophyll index [$CI_{red\ edge}$ = ($R_{nir}/R_{rededge}$) − 1] for the determination of linear regression coefficients (Ciganda, Gitelson & Schepers, 2009). The linear model allowed Chl_l estimation in both species, with a RMSD of less than 6 μg cm^{-2} in the Chl_l range from ~1 to 90 μg cm^{-2} (Gitelson, Vina, Ciganda, Rundquist & Arkebauer, 2005). Spectral reflectance measurements were collected approximately twice a week during the growing seasons of 2001 to 2005 and Chl_l of each leaf was retrieved by applying the calibrated $CI_{rededge}$ vs. Chl relationship. Predominantly green leaves were sampled, and estimates of total (green + senescent) Chl_l (Chl_t) was approximated as Chl_l × fg. This may underestimate Chl_t, particularly during significant degrees of senescence, where the "green" samples may already be partly senescing (Section 3.2). The uncertainty of the resulting in-situ Chl_l estimates is approximately 10%. The same uncertainty level is assumed for the LAI measurements and accounts for measurement errors and intra-field variability not captured by the selected measurement sites. The field measurements of LAI and Chl_l, which was found to be representative of the whole fields (Gitelson, Gritz & Merzlyak, 2003; Gitelson, Vina, et al., 2003; Gitelson et al., 2012), were interpolated to match the Landsat acquisition dates (Section 2.4) and compared to Landsat retrievals extracted within field-wide rectangles fitted to each site (540 m × 540 m for all sites) and subsequently averaged to produce a single value of LAI and Chl_l for each field.

2.6. Landsat data and REGFLEC setup

A total of 34 predominantly clear Landsat-5 TM and Landsat-7 ETM+ images (Fig. 4) were acquired over the 2001–2005 study period from the USGS EarthExplorer (http://earthexplorer.usgs.gov). All scenes were processed to standard terrain correction (Level 1 T), which provides systematic and geometric accuracy by incorporating ground
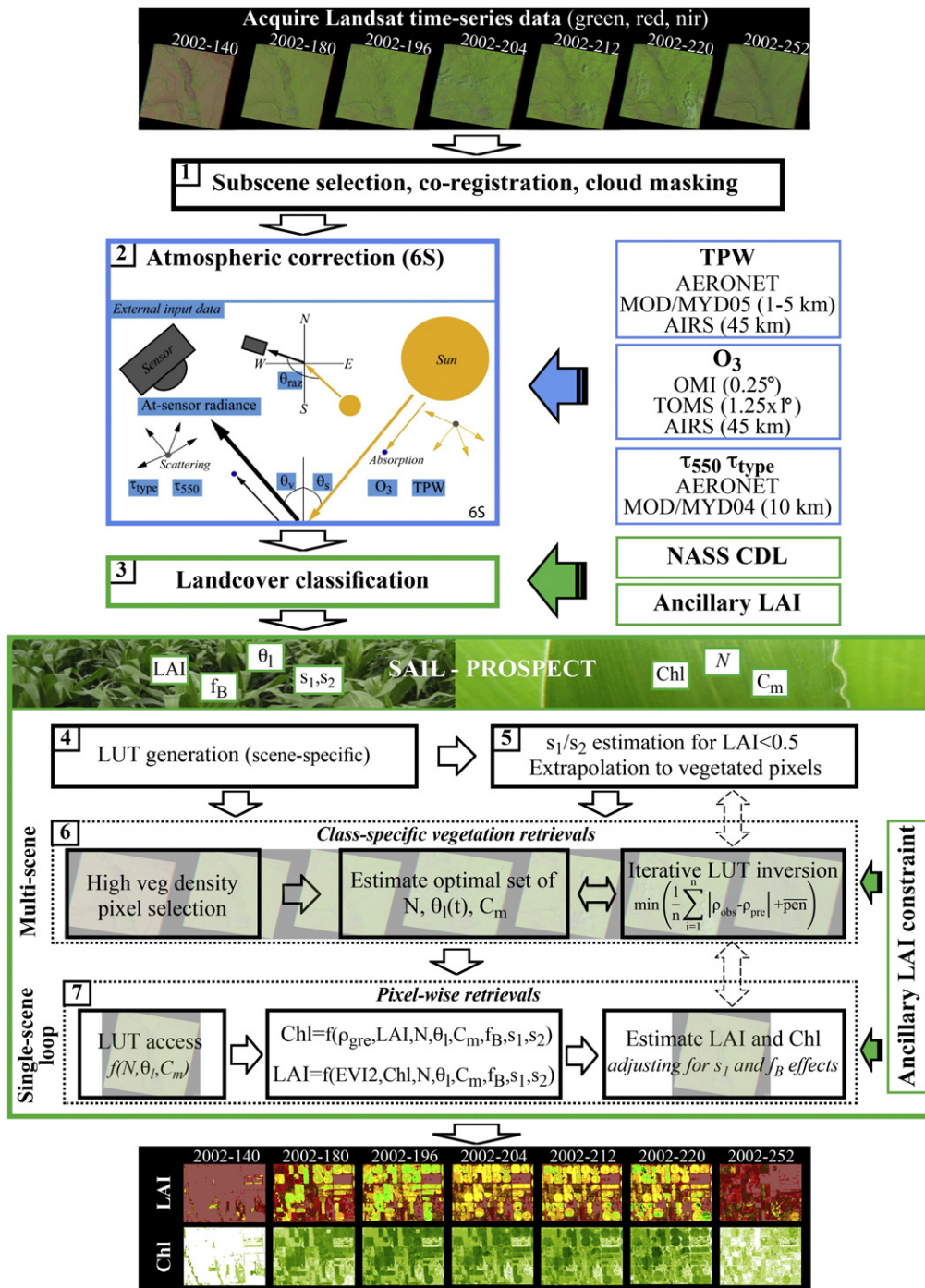
Fig. 2. Diagram of the REGularized canopy reFLECtance (REGFLEC) modeling system for translating at sensor radiance observations into leaf area index (LAI) and leaf chlorophyll content (Chl_l). REGFLEC combines atmospheric (6S), canopy (SAIL) and leaf (PROSPECT) models and adopts an iterative LUT-based inversion approach. The retrieval system implements multiple steps including automated processing streams based on readily available image-based sources, and incorporates ancillary information and spatio-temporal constraints for regularization purposes. In the provided minimization function (used in both step 5, 6 and 7), p_{obs} and p_{pre} represent observed and modeled spectral (green, red, near-infrared) reflectances, respectively and $\overline{pen}$ is a penalty operator. See Sections 2.1, 2.2 and 2.3 for parameter definitions and detailed methodology.

control points and a digital elevation model. The geodetic accuracy is typically within 30 m. The Mead sites are affected by striping in the Landsat-7 scenes due to scan line corrector failure of the ETM + sensor in May 2003 (Maxwell, Schmidt & Storey, 2007), but the data in between the stripes, that are approximately 4 pixels wide at this location within the Landsat swath, are still useful. The image digital counts were input to REGFLEC for further processing. For each year, the total number of scenes were first automatically co-registered and resized (the Mead sites are located in the center of the selected scene subset

of 1136 × 523 pixels – Fig. 3) and corrected for cloud contamination. At-sensor radiance data from each individual Landsat band (green, red and near-infrared) were atmospherically corrected following the internal REGFLEC procedure described in Section A.1. Aerosol size distribution (τ_{type}) was retrieved from the Konza EDC AERONET site, which is located ~250 km south of Mead.

REGFLEC was run with different configurations (Table 1) in order to evaluate the impact of PROSPECT model versions and regularization constraints on retrieval accuracies. The nominal REGFLEC run (R_{nom})
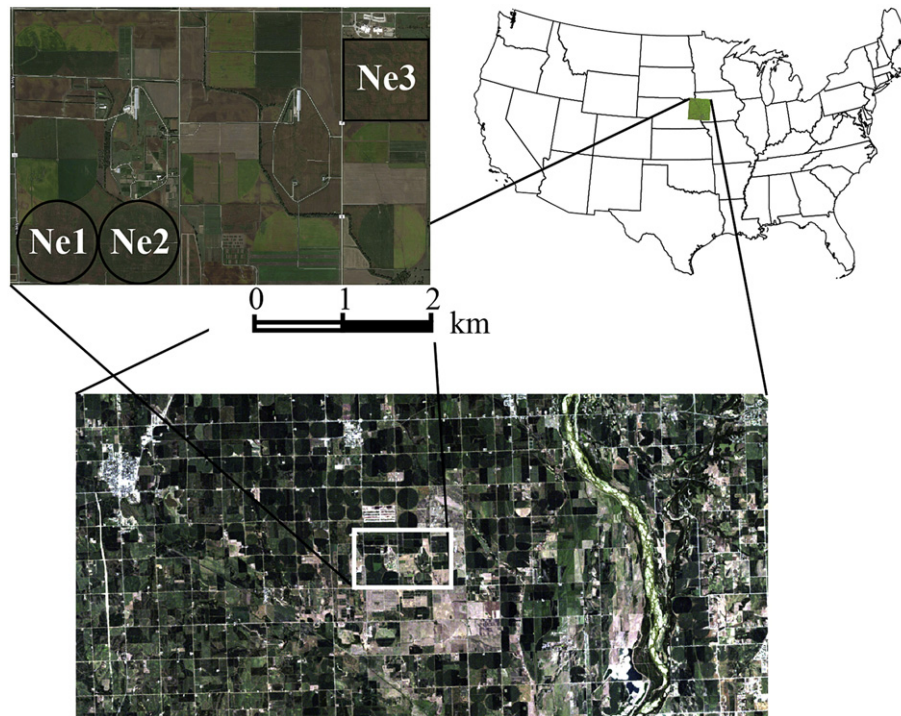
Fig. 3. Study area near Mead, Nebraska together with the location of the three field sites under continuous maize (Ne1) and maize-soybean rotation (Ne2, Ne3). The Landsat scene subset (shown) used as input to REGFLEC encompasses 1136 × 523 pixels, with the Mead sites located approximately in the center.

implements PROSPECT-4, soil background constraint (Section A.4), multi-scene constraint (Section A.5) and ancillary LAI constraint Section A.7). Five additional runs were configured on the basis of the nominal run configuration by changing each of the settings one at a time (Table 1). All runs used a year-specific land cover map generated by REGFLEC based on seasonal differences in phenology from ancillary LAI time-series data (Gao, Anderson, Kustas & Wang, 2012) and Cropland Data Layer products for Nebraska (Section A.2). Over the studied years, the adopted classification approach was found to facilitate proper class separation of the maize and soybean study sites.

3. Results and discussions

3.1. In-situ Chl_l and LAI variability

Fig. 5 displays averaged growing season time-series of measured Chl_l and LAI for maize and soybean fields at Mead. The time-series were
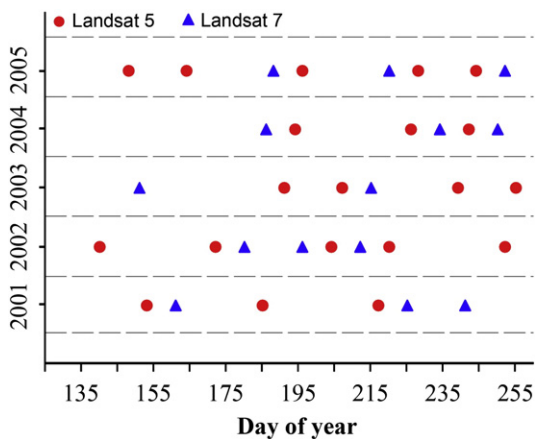
Fig. 4. Timing and frequency of acquired Landsat 5 and 7 scenes over the 2001–2005 study period used as input to REGFLEC.

constructed by crop-specific averaging of all available data points over the five-year study period (2001–2005) for the three sites (Ne1, Ne2, Ne3). As a result, the maize and soybean time-series were based on a total of 11 (Ne1: 2001–2005; Ne2 and Ne3: 2001, 2003, 2005) and 4 (Ne2 and Ne3: 2002, 2004) site-years, respectively. Fig. 5a shows overall dynamics of green LAI and fraction of senescent vegetation (f_B) in maize and soybean over the course of the growing season. Green-up starts earlier for maize (precedes soybean green-up by 20–30 days), the growth period is typically longer for maize than for soybean, and the maximum LAI of maize (~5) is higher than for soybean (~4). The large standard deviations (SD) and wide ranges are the result of significant interannual and inter-field variability caused by differences in environmental conditions and agricultural management practices (e.g. irrigated versus rainfed). This is also reflected in the time-series of Chl_l, particularly for maize, which is characterized by SD on the order of $\pm 10~\mu g~cm^{-2}$ throughout the growing season.

Maize is characterized by average Chl_l values on the order of $60~\mu g~cm^{-2}$ during peak LAI, whereas values between 30 and $40~\mu g~cm^{-2}$ are more characteristic for soybean (Fig. 5b). Similar differences in Chl_l between maize and soybean cultivars for healthy green vegetation have been reported in other studies (e.g. Daughtry, Walthall, Kim & Colstoun, 2000; Singh, Hoyos-Villegas, Ray, Smith &

Table 1
Overview of the different REGFLEC runs performed in this study, indicating the specific configurations (regularization constraints) and model choices of each run. P5, P4 and P3 represent different PROSPECT versions (Section 2.2).

Runs	P5	P4	P3	SC[a]	MC[b]	LC[c]
R_{nom}		X		X	X	X
R_{P5}	X			X	X	X
R_{P3}			X	X	X	X
R_{noSC}		X			X	X
R_{noMC}		X		X		X
R_{noLC}		X		X	X	

[a] Soil background constraint (section A.4).
[b] Multi-scene constraint (section A.5).
[c] Ancillary LAI constraint (section A.7).
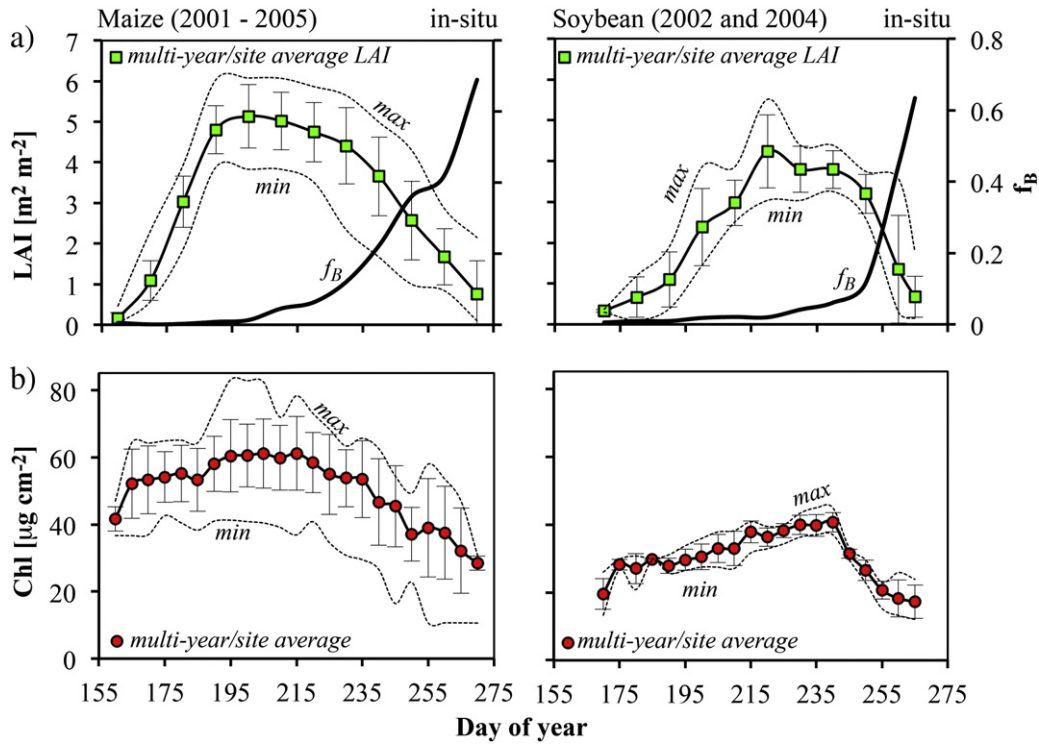
Fig. 5. Site (Ne1, Ne2, Ne3) and year (2001–2005) averaged time-series of measured (a) green LAI and (b) Chl$_l$ for maize and soybean fields at Mead, Nebraska. The bars represent standard deviations and degree of intra and inter-field variability over the five year period (2001–2005). Note that the maize and soybean time-series were based on a total of 11 (Ne1: 2001–2005; Ne2 and Ne3: 2001, 2003, 2005) and 4 (Ne2 and Ne3: 2002, 2004) site-years, respectively. The maximum and minimum observed LAI and Chl$_l$ values over the studied period are also indicated. In (a) the averaged measured canopy fraction of senescent leaf material (f$_B$) is plotted on the secondary y-axis.

Fritschi, 2013) and are a result of contrasting leaf structures and functionally different species types (i.e. C$_3$ versus C$_4$) with characteristic levels of peak Chl$_l$. Chl$_l$ typically increases during the green-up stage, reaching peak values in the reproductive stage, before declining again during late reproductive and senescence stages when green LAI also declines. The onset and magnitude of the late growing season decline in Chl$_l$ varies markedly from year to year, as evidenced by the large SD (Fig. 5b).

The availability of between 6 and 8 Landsat acquisitions each year that are distributed over the full growing season (Fig. 4) together with a wide range in measured LAI and Chl$_l$ responding to differences in plant species, plant development stage (green-up, reproductive, senescence), climate and management practices, allow for a thorough evaluation of the REGFLEC retrieval capacity.

3.2. Evaluation of LAI and Chl$_l$ retrievals (nominal run)

Fig. 6a compares REGFLEC retrieved Chl$_l$ against field-wide in-situ observations over a five-year period (2001–2005) that encompass different development stages (green-up, reproductive, senescence) of maize and soybean. These REGFLEC results are based on the nominal run configuration (R$_{nom}$), which embeds PROSPECT-4 and all three regularization constraints (SC, MC, LC) (Table 1). The impact of alternative REGFLEC configurations is discussed in Section 3.4.

REGFLEC predicts higher values of Chl$_l$ for maize (55 ± 5 μg cm^{-2}) than for soybean (30 ± 5 μg cm^{-2}) during green-up and reproduction (f$_B$ < 0.1), which is consistent with the in-situ measurements (55 ± 9 μg cm^{-2} and 32 ± 6 μg cm^{-2}, respectively) (Fig. 5b). The overall performance of REGFLEC in reproducing the dynamics of in-situ measured Chl$_l$ is characterized by a coefficient of determination (r^2) of 0.69, a mean bias error (MBE) of 0.04 μg cm^{-2}, and a root-mean-square-deviation (RMSD) of 8.42 μg cm^{-2}, which amounts to a relative RMSD of 19.1 % (Table 2, Fig. 6a). Several factors may affect the comparability

between satellite retrievals and in-situ measurements. For instance, in maize canopies, the vertical distribution of leaf Chl can be well described by a bell-shaped curve (Ciganda, Gitelson & Schepers, 2008), with maximal Chl$_l$ in leaves around the ear leaf located approximately 1–1.5 m from the top of the canopy (Ciganda, Gitelson & Schepers, 2012). The Landsat bands in the visible spectrum are characterized by relatively poor canopy penetration ability (due to high absorption) so that only a few leaf layers contribute to the canopy reflectance observed by the Landsat sensor. Consequently, the Landsat-based Chl$_l$ retrievals are likely to be lower than the in-situ measurements that represent maximal Chl$_l$ (Section 2.5), which is corroborated by a ~6% underestimation of maize Chl$_l$ (for f$_B$ < 0.1).

Discrepancies tend to be more pronounced during senescence (Fig. 6a), which for maize may partly be explained by enhanced complexity of the vertical Chl$_l$ distribution (Ciganda, Gitelson & Schepers, 2008; Gitelson, Peng, Arkebauer & Schepers, 2014) making direct comparisons between in-situ measurements and top of canopy satellite retrievals less viable. Another factor of uncertainty is the adopted multiplication of in-situ measured Chl$_l$ with the fraction of green vegetation to produce a total (green + senescent) Chl$_l$ (Chl$_t$) estimate comparable to that being retrieved by REGFLEC. This implicitly assumes that entirely green leaves were sampled and could result in underestimation of the actual Chl$_t$, particularly during advanced stages of leaf senescence. With these issues in mind, the Chl$_l$ retrievals appear reasonable and demonstrate the ability of REGFLEC in reproducing significant crop-specific seasonal and interannual Chl$_l$ variability in irrigated and rainfed maize and soybean fields (Fig. 5). The Chl$_l$ retrieval accuracies compare favorably to most results reported in other comparable studies on agricultural crops and grasses (e.g. Botha et al., 2007, 2010; Delegido, Vergara, Verrelst, Gandía & Moreno, 2011; Jacquemoud, Bacour, Poilve & Frangi, 2000), especially when considering the wide range in observed Chl$_l$ and crop conditions occurring over the five-year study period.
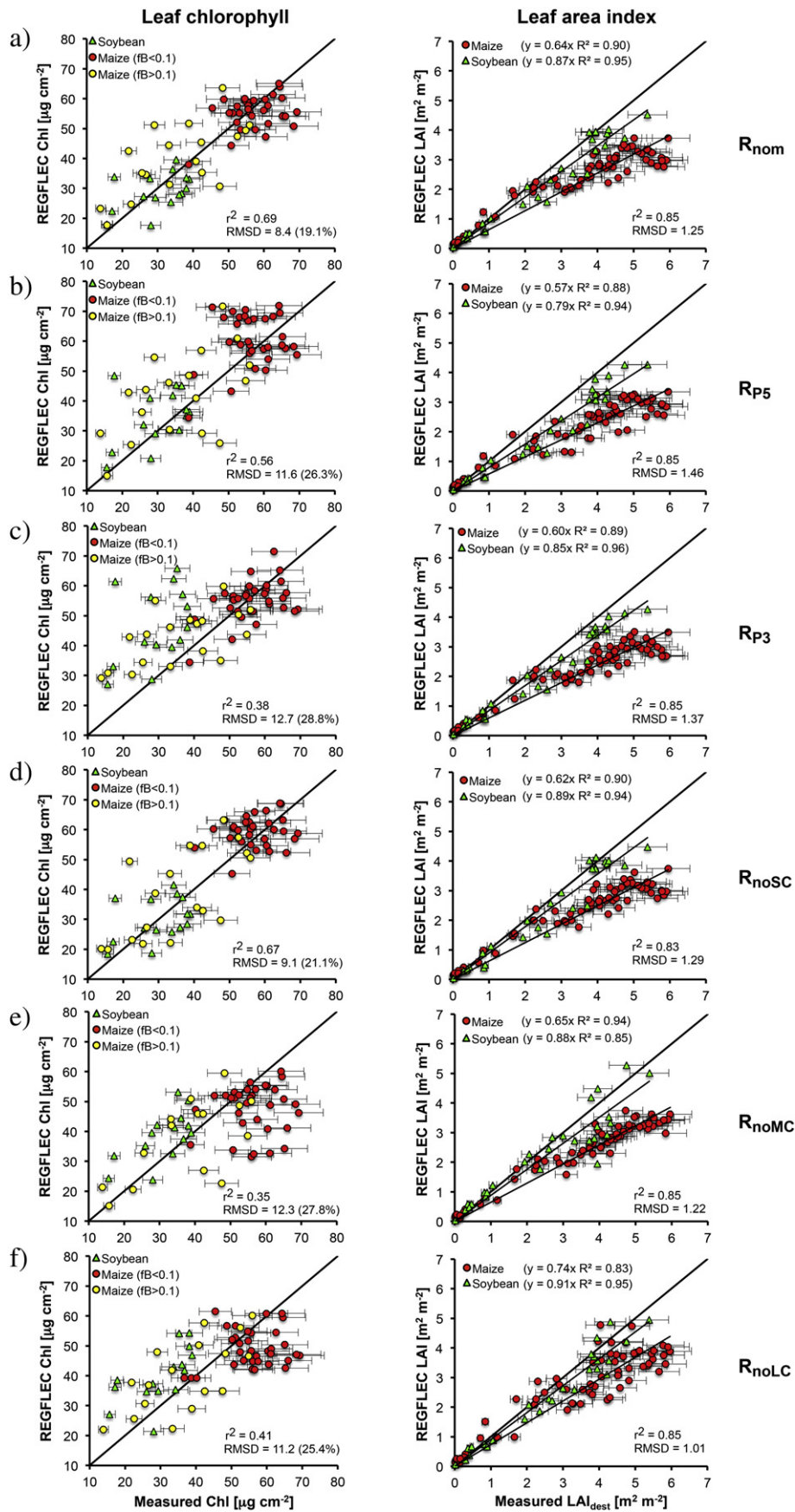
Table 2

Quantitative statistic measures of the performance of REGFLEC in estimating Chl [μg cm^{-2}] and LAI [m^2 m^{-2}] over maize and soybean using different setup configurations (Table 1). The REGFLEC retrievals were evaluated against in-situ measurements (n = 68 and 97 for Chl$_t$ and LAI, respectively) collected over 5 growing seasons (2001–2005) encompassing different development stages (green-up, reproductive, senescence). The last row shows the performance of the ancillary LAI dataset. The best performing statistic metrics are indicated in bold.

O is the mean of the in-situ measurements, S is the mean of REGFLEC retrievals, RMSD is the root-mean-square difference between model estimates and measurements, RRMSD is the relative RMSD (RMSD/O*100), MBE is the mean bias error (if positive REGFLEC overestimates measurements), and r^2 is the coefficient of determination. O, S, RMSD and MBE have units of μg cm^{-2}.

Runs		O	S	RMSD	RRMSD [%]	MBE	r^2
R$_{nom}$	Chl	44.1	43.9	**8.42**	**19.1**	**0.04**	**0.69**
	LAI	3.06	2.19	1.25	41.0	−0.88	**0.85**
R$_{P5}$	Chl	44.1	48.5	11.6	26.3	4.48	0.56
	LAI	3.06	1.90	1.46	47.6	−1.09	**0.85**
R$_{P3}$	Chl	44.1	49.8	12.7	28.8	4.79	0.38
	LAI	3.06	2.06	1.37	44.8	−1.00	**0.85**
R$_{noSC}$	Chl	44.1	46.3	9.31	21.1	1.93	0.67
	LAI	3.06	2.15	1.29	42.1	−0.91	0.83
R$_{noMC}$	Chl	44.1	42.5	12.3	27.8	−3.13	0.35
	LAI	3.06	2.21	1.22	39.9	−0.86	**0.85**
R$_{noLC}$	Chl	44.1	43.3	11.2	25.4	−0.66	0.41
	LAI	3.06	2.45	**1.01**	**32.8**	−0.62	**0.85**
Ancillary	LAI	3.06	2.14	1.25	41.1	−0.86	0.83

Table 3

Optimized year-specific class-invariant vegetation parameters for the study sites (Ne1, Ne2, Ne3) based on REGFLEC runs using the nominal configuration (Table 1). θ$_l$ is given for each site with an associated standard deviation to indicate the degree of spatio-temporal variability considered by the retrieval system (section A.5). In year 2001, 2003 and 2005 all three sites were under maize rotation.

Year	N		θ$_l$			C$_m$	
	Maize	Soybean	Ne1	Ne2	Ne3	Maize	Soybean
2001	3.5	-	67 ± 0.4	66 ± 0.8	68 ± 0.5	20	-
2002	3.9	1.3	66 ± 1.9	46 ± 5.8	52 ± 2.4	20	60
2003	3.6	-	66 ± 1.5	66 ± 1.1	68 ± 1.1	20	-
2004	3.3	1.3	65 ± 1.2	54 ± 1.9	56 ± 2.2	20	20
2005	3.8	-	69 ± 1.1	68 ± 1.3	70 ± 0.7	20	-

Degradation in model performances has often been observed during the leaf senescence stage (Bacour et al., 2002; Houborg & Boegh, 2008; Wang et al., 2005). Except for a few outliers, REGFLEC captures observed reductions in chlorophyll during the beginning to advanced stages of leaf senescence (f$_B$ = 0.1–0.6) (Fig. 6a). REGFLEC calculates Chl$_t$ by multiplication of green Chl$_l$ with pixel-specific values of (1 − f$_B$) (Section A.6). The onset of senescence is determined automatically for each class based on ancillary LAI (or EVI2) time-series data. During senescence, Chl$_l$ and LAI predictions are constrained by penalizing solutions that result in Chl$_l$ or LAI increases relative to retrievals from the preceding Landsat scene at corresponding pixel locations. This implementation proved effective at reproducing Chl$_t$ over the studied sites.

The overall performance of REGFLEC in reproducing the dynamics and magnitudes of in-situ measured LAI is characterized by a high correlation (r^2 = 0.85), whereas the RMSD (1.25 m^2 m^{-2}), relative RMSD (41 %) and MBE (–0.88 m^2 m^{-2}) indicate significant discrepancies (Table 2 and Fig. 6a). As ancillary LAI retrievals (Section A.7) were used to constrain the retrievals, the REGFLEC-based LAI will reflect the characteristics of that dataset to a large extent. Accordingly, the ancillary LAI estimates are also biased low (MBE = −0.86) and represented by similar levels of accuracy (RMSD = 1.26) (Table 2 and supplementary Fig. 1). The impact of the ancillary LAI constraint on the vegetation retrievals will be discussed in more detail in Section 3.4.

Independent linear regressions to the maize and soybean LAI data result in an excellent fit for soybean (r^2 = 0.95) with a 13% underestimation (slope = 0.87) (Fig. 6a). The destructively measured maize LAI on the other hand is being underestimated by 36 % (slope = 0.64) (Fig. 6a). Significant clumping has been observed in maize canopies (Demarez, Duthoit, Baret, Weiss & Dedieu, 2008), with the degree of clumpiness dependent on a complex interaction of leaf size, plant development stage, row spacing and view observation angle (Duthoit, Demarez, Gastellu-Etchegorry, Martin & Roujean, 2008; España, Baret, Chelle, Aries & Andrieu, 1998; López-Lozano, Baret, Chelle, Rochdi & España, 2007). According to España, Baret, Chelle, Aries and Andrieu (1998) for all phenological stages, clumpiness is more important for

near-nadir viewing directions (because of row effect; e.g. Landsat) and for fully-developed plants (high LAI), potentially yielding clumping factors as low as 0.6 (corresponding to a 40 % underestimation of effective LAI). Demarez, Duthoit, Baret, Weiss and Dedieu (2008) compared several methods of LAI estimation and found that effective LAI underestimated destructive LAI measurements in maize by 32 %, which corresponds closely to the skew reported in this study (y = 0.64x; Fig. 6a). The 4SAIL canopy reflectance model used in REGFLEC assumes homogeneous canopies with randomly distributed leaves and predicts an effective LAI (i.e. LAI × clumping) that will be lower than the true LAI in more heterogeneous and clumped canopies. A recent study also found that SAIL was not representing the spectral behavior of row crops such as maize, potatoes and sunflower well (Atzberger & Richter, 2012) and the large LAI underestimation over the Mead maize sites may indeed be partly attributable to differences between effective and true LAI caused by significant canopy clumping not properly accounted for in REGFLEC (i.e. SAIL) or in the ancillary LAI used as regularization constraint.

3.3. Class-specific vegetation retrievals

The LAI and Chl$_l$ predictive spectral relationships are strongly affected by model parameterizations, especially the values used for leaf structure (N), leaf inclination angle (θ$_l$) and dry matter content (C$_m$) (Fig. A1). A common approach is to fix these parameters using a priori information, typically taken from in-situ observations or from literature values. However, these vegetation parameters are not easily measured and approaches that rely on intensive field work for model calibration and parameterization are impractical from an operational stand point. REGFLEC adopts an approach independent of local calibration data that exploits the temporal and spatial radiometric information content of multiple satellite scenes (see Section A.5). In order for this approach to be meaningful, it is critical that the land cover map used as input to REGFLEC accurately separates individual crop types (such as maize and soybean), as any inter-class contamination may limit the utility of the inversion system for retrieving a unique set of optimized class-invariant vegetation parameters.

Table 3 lists the year-specific optimized parameter combinations for the study sites produced by the REGFLEC inversion system using the nominal configuration (R$_{nom}$). There are notable crop-specific differences in derived N and θ$_l$, ranging between 3.3–3.9 and 65–69° for maize and 1.3 and 46–56° for soybean, respectively. Note that the inversion considers modest spatio-temporal variability in θ$_l$ (Section A.5) as indicated by differences in the site-derived values (Table 3). The predictive green reflectance relationships are strongly influenced by N (Fig. A1a) and the high N values are the main cause for the high Chl$_l$

Fig. 6. Validation of REGFLEC total (green + senescent) Chl$_t$ and LAI retrievals against in-situ measured data from irrigated and rainfed agricultural fields over a 5 year period, demonstrating the impact of regularization constraints and model choices (Table 1). a) Nominal run configuration (R$_{nom}$), b) PROSPECT-5 run (R$_{P5}$), c) PROSPECT-3 run (R$_{P3}$), d) without soil background constraint (R$_{noSC}$), e) without multi-scene constraint (R$_{noMC}$), f) without ancillary LAI constraint (R$_{noLC}$). The error bars represent the assumed uncertainty (± 10%) of the in-situ measurements (Section 2.3).

levels characteristic of the maize retrievals (Fig. 6a). θ_l works in the opposite direction and increases in θ_l will significantly decrease estimated Chl_l for the same green reflectance value (Fig. A1a). Therefore, a low N (e.g. 1.5) along with a near-horizontal mean leaf inclination angle (e.g. $\theta_l = 20$) could result in similar levels of Chl_l as a high N (e.g. 3.5) and near-vertical leaf angle inclination (e.g. $\theta_l = 75$) (Fig. A1a). Variations in θ_l strongly affect spectral relationships used for LAI prediction (e.g. EVI2) (Fig. A1b), which limits the number of feasible N and θ_l combinations, as only a few will minimize the overall difference between modeled and observed spectral reflectances (green, red and near-infrared), while assuring that Chl_l and LAI remain within a realistic range.

Maize and soybean have contrasting leaf structures and canopy architectures, with soybean tending towards a more horizontal leaf angle distribution (LAD) whereas the LAD for maize is more spherical (Gitelson, Vina, Ciganda, Rundquist & Arkebauer, 2005). These tendencies are supported by the contrasting N retrievals and lower values of θ_l retrieved over Ne2 and Ne3 during soybean rotation years (2002 and 2004) (Table 3). N represents the leaf anatomy and cannot be directly measured. It has been determined by inverting the PROSPECT model using databases of measured leaf reflectance and transmittance spectra (e.g. Hosgood et al., 1995) and the typically accepted range of N is on the order of 1–3 (Feret et al., 2011; Jacquemoud & Baret, 1990), although a verifiable set of species-specific values does not exist. Clearly, the derived N values for maize are outside the 'realistic' range of values reported in the literature, but expanding the allowed N range (1–4) was deemed necessary in order to achieve realistic Chl_l values for maize and properly match observed spectral signatures. In Richter, Atzberger, Vuolo, Weihs and D'Urso (2009) PROSPECT-SAIL (PROSAIL) failed to invert over maize and Atzberger and Richter (2012) demonstrated that forward simulations with PROSAIL using field measured biophysical parameters as input did not match observed spectral signatures of maize, as the 1D turbid medium SAIL model does not take into account row effects, shading and heterogeneous canopy architectures. Issues with the PROSPECT calibration may also impair the capability of PROSAIL to properly simulate observed canopy spectra (Section 3.4.1). Another potential source of uncertainty comes from light scattered at the surface of leaves; this partly polarized portion of the reflected light does not enter the leaf and thus conveys no direct information about its interior (e.g. leaf biochemistry). Polarization measurements may be needed to effectively correct for this confounding factor (Vanderbilt, Grant & Daughtry, 1985).

Model uncertainties and limitations of this sort may severely reduce LAI and Chl_l retrieval accuracies and caution should be exercised when using field measured data or 'realistic' ranges reported in the literature for model parameterization. This is particularly true for N, as it strongly affects Chl_l and cannot be measured directly. As such, it may function more conveniently as a model calibrator that is being optimized to better match observed and modeled reflectance spectra (Houborg & Anderson, 2009). By doing this, SAIL and/or PROSPECT model limitations are being compensated for by N adjustments, which could result in erroneous leaf reflectance and transmittance spectra. At least for the studied area, these adjustments do result in realistic LAI and Chl values being simulated by SAIL-PROSPECT (R_{nom}) for both soybean and maize. Ideally, a more physically realistic canopy reflectance model with consideration of 3D effects (e.g. DART; Gastellu-Etchegorry, 1996) should be adopted, but the enhanced complexity is an obvious limitation for satellite-based applications, particularly given the limited radiometric and spatial information content of the Landsat sensors. Multi-sensor approaches and future satellite systems may offer opportunities for investigating this further.

3.4. Impact of configuration and regularization constraints

In physically-based frameworks, the accuracy of vegetation retrievals depend on the quality and radiometric information content

of the input radiance data, the quality of the atmospheric correction, the physical realism and parameterization of the models used, and techniques applied for regularizing the inversion process. The impact of PROSPECT model version and three different regularization constraints (Table 1) on LAI and Chl_l retrieval accuracies are evaluated below. The output from each REGFLEC configuration is compared to in-situ measurements in Fig. 6b–f, with statistic measures of performance listed in Table 2. Fig. 7 provides time-series and difference maps of Chl_l and LAI over the studied fields during 2002 to showcase the impact of REGFLEC configurations in a spatial context.

3.4.1. Influence of PROSPECT version

REGFLEC was run with 3 different versions of PROSPECT (P3, P4 and P5) characterized by different chlorophyll absorption coefficients (Fig. 1) and refractive indices. P4 and P5 are based on the same experimental dataset of leaf biochemical and optical properties, but P5 allows separate treatment of chlorophylls and carotenoids. However as the carotenoids content was unrealistically set to zero for these analyses, the results cannot be used to assess the actual validity of PROSPECT-5, albeit providing useful insights into the impact of PROSPECT calibration. The choice of PROSPECT model version has a significant impact on the Chl_l retrieval performance with P4 (R_{nom}) performing best (RMSD = 8.42 $\mu g\ cm^{-2}$, $r^2 = 0.69$), followed by P5 (R_{P5}) (RMSD = 11.6 $\mu g\ cm^{-2}$, $r^2 = 0.56$) and then P3 (R_{P3}) (RMSD = 12.7 $\mu g\ cm^{-2}$, $r^2 = 0.38$) (Table 2, Fig. 5a–c). P4 is characterized by greater chlorophyll absorption than P3 and P5 in the 400–550 nm region (Fig. 1a), which results in lower canopy reflectance in the blue and green bands of the Landsat sensor for a given Chl_l (Fig. 1b). This implies that for the same model parameterization, the inversion of the same canopy reflectance spectra will yield an increasingly higher Chl_l value when changing from P4 to P5 to P3. Accordingly, the use of both P5 and P3 caused REGFLEC to overestimate Chl_l (MBE = 4.48 and 4.79 $\mu g\ cm^{-2}$, respectively) (Table 2).

The generally higher Chl_l levels simulated with R_{P5} and particularly R_{P3} are clearly evident in the time-series maps for the 2002 growing season (Fig. 7a). When looking at crop specifics, R_{P3} does reasonably at reproducing the magnitudes and variability of maize Chl_l (Fig. 6c) and interestingly does so based on a more 'realistic' class-specific parameter combination ($N \sim 1.0$, $\theta_l \sim 50$, $C_m = 80\ g\ m^{-2}$) (Table 3). However, R_{P3} has difficulty reproducing the lower Chl_l values characteristic of soybean, which are being overestimated by ~50% on average (Fig. 6c). In the R_{P3} simulation N hits the lower bound (=1.0) for soybean and still predicts relatively high Chl_l (~50 $\mu g\ cm^{-2}$ on average), suggesting chlorophyll absorption is too low when produced by this calibration. R_{nom} (using P4) on the other hand, provides a much better approximation of low Chl_l (e.g. those characteristic of soybean). However, P4 needs a wider N range to reproduce the high Chl_l characteristic of maize, as discussed in Section 3.3. The Chl_l simulated with P5 can be modulated by changing the carotenoid content and it is likely that a real test with P5 (Car > 0) could result in improved estimation of Chl_l, particularly if hyperspectral information is available for properly discriminating chlorophyll and carotenoid pigments (Blackburn, 2007; Gitelson, Keydan & Merzlyak, 2006; Sims & Gamon, 2002). The LAI retrieval accuracy also decreases when using P3 or P5 in place of P4 (MBE increases from −0.88 to ~−1.0), although the impact is modest as the ancillary LAI constraint was active in all three simulation runs (Fig. 6a–c).

These results highlight the strong sensitivity of vegetation retrievals (particularly Chl_l) to the adopted refractive index spectrum and specific absorption coefficients for pigments in PROSPECT and there is a need for continued research to improve the modeling of leaf reflectivity for application to both monocots (maize) and dicots (soybean) (Comar et al., 2014). While the blue spectrum holds information valuable for LAI and Chl_l detection (Huete et al., 2002; Hunt, Daughtry, Eitel & Long, 2011), the large differences in calibrated absorption coefficients in the blue spectrum (Fig. 1) adds to the significant uncertainties with
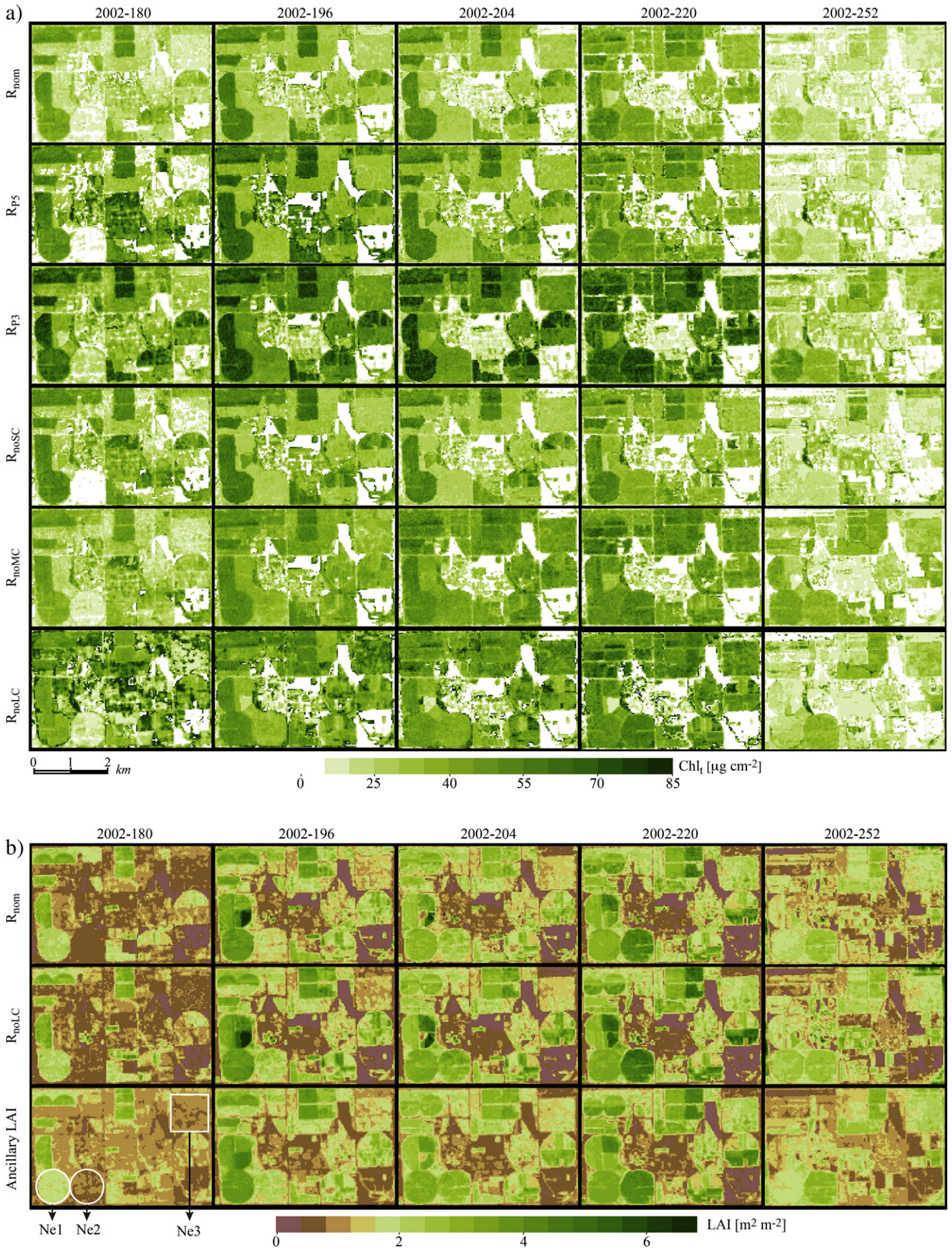
Fig. 7. Maps of total (green + senescent) (a) Chl_t and (b) LAI over the studied fields in 2002, demonstrating the impact of REGFLEC configuration (Table 1).

using this wavelength region in remote sensing applications (Fensholt, Sandholt & Stisen, 2006). The predictive ability of PROSPECT-4 and 5 chlorophyll retrievals are reportedly on the order of 10 μg cm^{-2}, while failing completely for the widely used LOPEX experimental dataset (RMSD ~ 30 μg cm^{-2}, attributed to a bias) (Feret et al., 2008), highlighting the significant challenges and uncertainties associated with applying physically-based approaches. Clearly, a high degree of realism in process description and robust knowledge of the refractive index and specific absorption coefficients is fundamental for reliable quantification of foliar pigments when inverting a canopy reflectance model (Feret et al., 2008, 2011; Le Maire, François & Dufrêne, 2004).

3.4.2. Impact of spatio-temporal constraints

Low Chl$_l$ and LAI estimation accuracies have been attributed to soil background interference in a number of studies (Botha, Leblon, Zebarth & Watmough, 2010; Gobron, Pinty & Verstraete, 1997). REGFLEC separates the estimation of the background signal from the retrieval of class-specific canopy parameters to reduce the number of free parameters and minimize potentially confounding influences of the background reflectance signal (Section A.4). The accuracy of the established soil parameter maps (s$_1$ and s$_2$) depend on the number and distribution of soil pixels (LAI < 0.5) in the image and the ability to reliably fill any spatial gaps using maps of s$_1$ and s$_2$ generated during sparse vegetation cover conditions. If previously generated soil parameter maps are not used as a constraint (R$_{noSC}$), spatial gaps (LAI > 0.5) will be filled based on the extrapolation of s$_1$ and s$_2$ values from existing soil pixels in the given scene. The mean of R$_{noSC}$ Chl$_l$ retrievals (46.3 μg cm^{-2}) is higher than for R$_{nom}$ (43.9 μg cm^{-2}), and the impact of the soil background constraint on Chl$_l$ is clearly visible in the scatter plots (Fig. 6a and d) and maps (Fig. 7a), particularly over intermediate vegetation coverage (Fig. 7b). It is also reflected in the Chl$_l$ retrieval capacity (RMSD decreases from 8.42 to 9.31 μg cm^{-2}, Table 2). Establishing the soil background signal below a vegetation canopy based on signals from neighboring or pre-growing season sparsely vegetated pixels is associated with large uncertainties, as the background reflectance signal responds to changes in soil texture, soil moisture and ground cover conditions, which may vary significantly in space and time. Irrigation effects constitute an additional complication. While physically-based implementations of the soil moisture effect on the soil reflectance spectra exist (Verhoef & Bach, 2007), the required detailed spatial information is not readily available. Further detailed investigations are needed to develop improved image-based approaches to take these issues into account.

The multi-scene constraint (Section A.5) simultaneously incorporates spectral reflectance observations over intermediate to dense vegetation from multiple Landsat scene acquisitions over the growing season to derive an optimal set of class-specific (and seasonally fixed) vegetation parameters. When this constraint is not invoked (R$_{noMC}$), the retrieval of class-specific vegetation parameters (N, θ$_l$ and C$_m$) is undertaken independently for each scene (if a sufficient amount of intermediate to dense vegetation pixels exist) allowing for unconstrained fluctuations in N, θ$_l$ and C$_m$ over the course of the growing season for a given land cover class. The importance of the multi-scene constraint is clearly illustrated by the R$_{noMC}$ validation statistics (Table 2, Fig. 6e), with r^2 decreasing to 0.35 and the RMSD increasing to 12.3 μg cm^{-2} for Chl$_l$. The reduced retrieval accuracy is partly the result of occasional temporal jumps in N, such as in 2003 when retrieved N changed from 1.5 on DOY 191 to 3.75 on DOY 207, which results in unrealistic temporal Chl$_l$ behavior. The temporal Chl$_l$ dynamics are also affected over the 2002 growing season and the Chl$_l$ of the maize (Ne1) and soybean (Ne2, Ne3) sites is not well discriminated (e.g. approximately similar levels on DOY 220) (Fig. 7a). The multi-scene constraint is needed to arrive at well-constrained class-specific vegetation parameters and avoid temporal variations in N and C$_m$ over the growing season for a specific land cover class.

The plot of measured Chl$_l$ against retrievals without the ancillary LAI constraint (R$_{noLC}$) (see Section A.7) shown in Fig. 6f is characterized by significantly more scatter (r^2 = 0.41 and RMSD = 11.2 μg cm^{-2}) compared to retrievals constrained by ancillary LAI (r^2 = 0.71 and RMSD = 8.42 μg cm^{-2}) (Fig. 6a). This is not unexpected, as LAI and Chl$_l$ have a mutually compensating effect on canopy spectra making accurate separation difficult. Large differences in retrieved Chl$_l$ are especially evident over sparsely vegetated pixels (Fig. 7a and b). Chl$_l$ retrievals based on Landsat data are characterized by large uncertainties for low LAI (LAI < 1) due to decreasing spectral sensitivity and increasing influence of confounding factors, especially LAI and soil background (Houborg, Anderson & Daughtry, 2009). Thus, minor changes in derived LAI and soil reflectance may result in markedly different Chl$_l$ retrievals and this issue becomes especially evident when LAI is not being constrained, as illustrated by the enhanced intra-field Chl$_l$ variability in the R$_{noLC}$ output for DOY 180 over low LAI pixels (Fig. 7a and b).

Surprisingly, unconstrained (R$_{noLC}$) LAI retrievals are characterized by the highest estimation accuracies (RMSD = 1.01) and reduced underestimation of destructively measured LAI (MBE = −0.66) (Table 2, Fig. 6f). On average, the simulations underestimate soybean and maize LAI by 9% and 26%, respectively (Fig. 6f), which is a considerable improvement over the constrained LAI validation results (Fig. 6a–e, Table 2). The ancillary LAI dataset used in this study (Gao, Anderson, Kustas & Wang, 2012) produces MODIS consistent LAI at the Landsat spatial scale by relating LAI retrievals at the MODIS 1 km scale to co-incident Landsat surface reflectances based on a regression tree approach. Given the coarse resolution of the MODIS sensor, high LAI values in sub-pixel agricultural fields are likely to be under-sampled by this approach, causing under-estimation of actual LAI (Gao, Anderson, Kustas & Wang, 2012; Guindin-Garcia, Gitelson, Arkebauer, Shanahan & Weiss, 2012). While in-situ LAI observations may be incorporated into the training process to effectively reduce under-sampling of high LAI values (Gao, Anderson, Kustas & Houborg, 2014) or used for developing accurate empirical LAI prediction algorithms (Gitelson, Wardlow, Keydan & Leavitt, 2007; Viña, Gitelson, Nguy-Robertson & Peng, 2011), these implementations have limited utility for more operationally oriented applications. In addition, SAIL outputs an effective LAI that may diverge considerably from the true LAI due to foliage clumping effects and it is important that the ancillary LAI used as a constraint complies with this definition.

The REGFLEC unconstrained LAI retrievals produce spatial and temporal patterns that are similar to those recorded in the ancillary LAI dataset (Fig. 7b), with generally modest differences in LAI magnitudes (see also supplementary Fig. 1). Nevertheless, the impact on retrieved Chl$_l$ is visibly significant over the 2002 growing season, notably for the soybean fields (Ne2 and Ne3), where Chl$_l$ typically increases by 10–25 μg cm^{-2} compared to R$_{nom}$ simulations (Fig. 7a). Variations in retrieved Chl$_l$ may partly be the result of spatio-temporal dynamics in θ$_l$ considered by R$_{nom}$ but not R$_{noLC}$ (Section A.5). This highlights the strong sensitivity of the Chl$_l$ retrievals to even small changes in confounding factors.

4. Summary

The achievable accuracy of joint LAI and Chl$_l$ retrieval was examined within a regularized model inversion system, using standard broad spectral bands (green, red and near-infrared) available from an operational remote sensing system. A fundamental property of the REGFLEC model is the ability to retrieve both LAI and Chl$_l$ directly from at-sensor radiances using a fully integrated system of radiative transfer models that can be applied over most regions without the need for site-specific calibration, using information extracted entirely from image-based and readily available datasets. As part of a iterative LUT-based inversion approach, REGFLEC diagnoses a suite of predictive LAI and Chl$_l$ spectral reflectance relationships, which are specific to each scene acquisition (view and illumination geometry) and dependent on

land cover class, leaf structure, canopy architecture and soil background conditions. Validation against in-situ data collected over maize and soybean sites in central Nebraska over a 5-year period demonstrated that it is feasible to retrieve LAI and Chl_l from Landsat data with good accuracy when the inversion process has been properly regularized.

The shape of canopy spectra depend on many internal and external factors that may easily confound the detection of the signal attributed to a single biophysical property such as LAI or leaf Chl. A physical model is required to properly account for these confounding factors and derive meaningful spectral relationships. However, physically-based systems are sensitive to uncertainties in model parameterization and limitations in the description of physical processes. In this study, the Chl_l predictability strongly depended on the adopted refractive index spectrum and specific absorption coefficients for pigments in PROSPECT, and it was necessary to significantly expand the allowed range of the leaf structure parameter (N) in order to properly match observed spectral signatures and achieve realistic Chl_l for maize with PROSPECT-4. Importantly, applications of SAIL-PROSPECT using field measured data or 're-alistic' parameter distributions as input can lead to biased Chl_l results due to calibration issues like this.

The ill-posed nature of model inversion, which results in different combinations of model parameters corresponding to almost identical spectra, constitutes an additional complication. The limited information carried by the radiometric signal of space based platforms calls for the application of novel spatio-temporal regularization techniques to introduce additional information useful for guiding the inversion process in the right direction. The use of ancillary LAI, based on downscaled MODIS LAI, was shown to be effective at regularizing the ill-posed inverse problem, with improved separation of LAI and Chl_l effects on observed reflectance spectra. Likewise, establishing the soil background signal for vegetated pixels based on a pre-growing season satellite scene and imposing a multi-scene constraint for the retrieval of class-specific vegetation parameters, lead to improved robustness of the retrievals. Although the applied temporal and spatial constraints proved effective, reliable extraction of Chl_l magnitudes from satellite observed top of canopy reflectances remains extremely challenging. Variations in atmospheric conditions, vegetation structure and soil background, in addition to model uncertainties, all complicate the detection of relatively subtle differences in canopy reflectance resulting from changes in Chl_l. Accurate detection of absolute Chl_l is essential for meaningful utilization within process-based land surface models for parameterization of photosynthetic capacity (Houborg, Cescatti, Migliavacca & Kustas, 2013) and for precision farming applications requiring consistent information on leaf nitrogen status. In order to ensure the retrieval of consistent and realistic Chl_l levels on a crop-specific basis, a set of land cover based nominal Chl_l values (representative of optimal unstressed conditions) could potentially be incorporated to guide the inverse retrieval of class-specific vegetation parameters (favoring best fit solutions that provide the closest approximation to the nominal Chl_l). This would require information on crop type and associated nominal Chl_l from an extensive literature review and existing databases (e.g. TRY; Kattge et al., 2011).

Accurate retrieval of vegetation biophysical properties is complicated by the competing balance between the physical realism of models that describe the transfer and interaction of radiation inside the canopy and the need of simplified descriptions for effective parameterization in a remote sensing context. The homogeneous canopy assumption of a turbid medium canopy reflectance model like 4SAIL may not be appropriate for heterogeneous canopies with more complex structures and significant shadowing effects (Schlerf & Atzberger, 2006) and will lead to LAI underestimation in case of canopy clumpiness (as shown for maize in this study). However, the simplification is often required to reduce the dimensionality of the inversion process (Goel, 1988). Recognizing that effective LAI is being retrieved, improved approximations of true LAI may be achieved by division with vegetation clumping index values derived from multi-angular data (Pisek et al., 2013). A

key objective for future research is to investigate how the type, complexity and physical realism of canopy reflectance models may affect the retrieval accuracies within the framework of REGFLEC. Additional model choices such as NADIM (Gobron, Pinty, Verstraete & Govaerts, 1997), 4SAIL2 (Verhoef & Bach, 2007), and DART (Gastellu-Etchegorry, 1996) are in the process of being implemented for this purpose.

Future applications of REGFLEC will focus on implementing additional spectral bands in order to increase the amount of information used in the inversion process. Indices based on bands in the red-edge region (Dash & Curran, 2007; Gitelson, Gritz & Merzlyak, 2003) are characterized by improved sensitivity over the full range of chlorophyll values and reduced sensitivity to confounding factors. Additional bands on the near-infrared plateau would be helpful for improved detection of leaf senescence. Hyperspectral data streams have the potential to enhance Chl retrieval capabilities even further (e.g. Malenovský et al., 2013), although careful attention to confounding factors remains a necessity (Baret, 1991). Unfortunately, super- or hyperspetral information is not available or being freely distributed on a routine basis by the existing suite of space satellites. The pair of Sentinel-2 satellites from the European Space Agency, with the first satellite scheduled to launch in 2015, will be delivering super-spectral data at resolutions down to 10 m with an exceptional revisit capability of 2–5 days once both satellites are in orbit, which is likely to be highly beneficial for joint LAI and Chl_l detection within the framework of REGFLEC, significantly advancing the ability to monitor plant physiological conditions (Clevers & Gitelson, 2013; Clevers & Kooistra, 2012; Schlemmer et al., 2013). In the meantime, continuation with Landsat data has been secured with the successful launch of Landsat-8. Nevertheless, with Landsat alone, given a 16-day revisit time that can be significantly lengthened due to cloud contamination, the temporal sampling frequency is rarely sufficient to properly resolve time-varying dynamics in vegetation functioning. In the present study, even with two Landsat satellites available, temporal gaps of up to 30 days occurred (Fig. 4). In order to improve temporal sampling frequency, data from multiple instruments may be used synergistically (e.g. Landsat, SPOT) or the spatial detail from high spatial resolution sensors such as Landsat may be fused with high frequency observations from spatially coarse resolution sensors such as MODIS (Gao, Masek, Schwaller & Hall, 2006).

To conclude, physically-based joint retrieval of LAI and Chl_l from Landsat observed reflectances, independent of local calibration data, remains a challenging task due to the ill-posed nature of model inversion and the limited information carried by the radiometric signal. Continued development of image-based regularization techniques is needed to mitigate this ill-posed inverse problem (i.e. properly discriminate contributions from the atmosphere, canopy and soil) and achieve higher estimation accuracies. Clearly, additional advances in the retrieval of canopy biophysical and leaf biochemical constituents for reliable detection of rapid changes in vegetation health and photosynthetic functioning will require innovative (and potentially synergistic) use of existing remote sensing data within physically realistic canopy reflectance models as well as the ability to exploit the enhanced spectral and spatial capabilities of upcoming satellite systems. Relating satellite-retrieved leaf-level biochemical constituents to key carbon-related parameters (e.g. photosynthetic capacity, light-use-efficiency) in a consistent manner for integration into land surface models is another important but challenging objective for future research.

Acknowledgements

Appendix A. REGFLEC description

The REGFLEC multi-step retrieval and regularization methodology (Fig. 2) is described in detail below.

A.1. Data preprocessing and atmospheric correction (step 1 and 2)

The current version of REGFLEC requires growing season time-series of Landsat terrain corrected (Level 1 T) products as input. Built in processing routines handle scene sub-setting, co-registration and cloud masking. Clouds and cloud shadows are automatically detected using the Fmask object-based approach (Zhu & Woodcock, 2012), which has proven highly effective, with overall detection accuracies on the order of 96 %. The preprocessed Landsat images of at-sensor radiances are atmospherically corrected using 6S (Section 2.1). For Landsat imagery, the sensor view zenith angle (θ_{vz}) may vary between $-7.5°$ and $7.5°$, and the important spatial variation in θ_{vz} is extracted automatically from the imagery using information on the scene orientation angle and the distance to the scene center meridian. A REGFLEC Graphical User Interface (GUI) includes routines for download and on the fly processing of atmospheric state and ancillary data from various satellite and ground-based sources (Fig. 2). Surface elevation may be retrieved from the GTOPO30 global digital elevation model at approximately 1 km resolution. Point-specific τ_{550}, total precipitable water (TPW) and aerosol size distribution can be retrieved from AERONET data (Holben et al., 1998). In this case, REGFLEC will search for nearby AERONET sites and handle all data access and processing needs. Spatially distributed τ_{550} data at 10 km resolution can be acquired from the MODIS aerosol product (MOD/MYD04) and TPW at 1 or 5 km resolution can be retrieved from the MODIS water vapor products (MOD/MYD05) or at 45 km resolution from the Atmospheric Infrared Sounder (AIRS) standard retrieval product by interfacing directly with the respective data distribution servers. O_3 is also retrievable from AIRS data. Alternative O_3 sources embedded within REGFLEC include the Total Ozone Mapping Spectrometer (TOMS) ($1.25 \times 1°$ resolution) and the Aura Ozone Monitoring Instrument (OMI) ($0.25°$ resolution). The REGFLEC GUI conveys quality and uncertainty information, and it is possible to combine the various products for gap-filling purposes.

A.2. Land cover classification (step 3)

A land cover map that accurately separates individual crop classes represents a critical component of the REGFLEC retrieval technique, although knowledge of the actual cover types is not currently a requirement. An embedded and automated land cover classification scheme performs class separation based in part on an unsupervised ISODATA classification technique (Tou & Gonzalez, 1974) and Normalized Difference Vegetation Index (NDVI) time-series data, thereby using differences in phenology to distinguish functionally different cover types. An ISODATA classification with input of cloud-screened atmospherically corrected NDVI images is first run to generate a large number (~100) of initial classes. Time-series correlation coefficients (r^2) and root-mean-square-deviations (RMSD) are computed between class-averaged NDVI time-series, with these metrics then used to combine classes with similar phenology ($r^2 > 0.92$) and NDVI magnitudes (low RMSD). If ancillary LAI is used to constrain the vegetation parameter retrievals (Section A.7), it is possible to use the independent LAI time-series data in place of NDVI as a proxy for phenology. Additionally, within the conterminous USA, the classification may make use of Cropland Data Layer (CDL) products from the U.S. Department of Agriculture National Agricultural Statistics Service (http://www.nass.usda.gov/research/Cropland/SARS1a.htm) to guide the grouping of iso-classes. The CDL classifies U.S. crop cover types using satellite imagery from the Advanced Wide Field Sensor (AWIFS) and Landsat, together with a variety of

ancillary datasets and ground truth data (Han, Yang, Di & Mueller, 2012). The spatial resolution of most CDL data is 30 m and covers all 48 adjoining states starting from 2009, although many states have yearly CDL data back to 1997. The full CDL dataset can be automatically accessed within REGFLEC and used either as a stand-alone land cover classification or as ancillary input to the embedded land cover classification routine.

A.3. LUT generation (step 4) and access

LUTs of spectral reflectances and VIs (Table A1) are generated by running SAIL-PROSPECT (Section 2.2) in forward mode for a given view and illumination geometry (θ_{sz}, θ_{vz}, θ_{az}, θ_{saz}) over a wide parameter distribution space (Table A2). The ranges adopted for LAI and Chl$_l$ (0–8 and 10–90 $\mu g\ cm^{-2}$, respectively) are expected to cover the variability observed in most ecosystems. The LUTs consist of 8 dimensions, as a reflectance value must be stored for all possible combinations of each LAI, Chl$_l$, N, θ_l, f_B, C_m, s_1, and s_2 entry. For some parameters, the LUTs are only computed for a few entries to reduce the computational demand of the LUT generation (total number of parameter combinations = 636480/LUT). The parameter range for N and θ_l have been set particularly wide (1–4 and 5–80°, respectively) to make the system applicable to a wide range of leaf structures and canopy architectures. A previous study using REGFLEC (Houborg & Anderson, 2009) indicated that these model parameters may function more as internal calibrators of the model system, compensating for input reflectance errors and model deficiencies, causing deviations from a 'realistic' set of cover specific parameter values while still maintaining reliable LAI and Chl$_l$ estimations. This tendency is discussed in greater detail in Section 3.3.

The LUTs are used in forward mode for LAI/Chl$_l$ estimation (as a function of observed reflectances) and in inverse mode for spectral reflectance estimation (as a function of LAI/Chl$_l$). Chl$_l$ and LAI spectral relationships are established for given parameter entries (N, θ_l, f_B, C_m, s_1, and s_2) by fitting a polynomial or exponential equation to the modeled reflectance or VI value at each Chl$_l$ and LAI entry, respectively. Parameter entry values that fall in between the respective LUT entries (Table A2) are considered by linearly interpolating between bounding parameter values when accessing the LUTs (Houborg, Anderson & Daughtry, 2009), which makes the results less sensitive to the specified parameter entries.

When using Landsat data, green band reflectance (R$_{green}$) relationship are used for Chl$_l$ prediction. Clearly, modeled R$_{green}$ responds significantly to changes in Chl$_l$ (Fig. A1a) and for dense cover conditions (LAI > 2.5), Chl$_l$–R$_{green}$ relationships are largely unaffected by further increases in LAI and changes in soil background conditions due to a very low leaf transmittance in the green spectrum (Houborg, Anderson & Daughtry, 2009). However, at high vegetation densities, Chl$_l$–R$_{green}$ relationships are highly sensitive to changes in both N and θ_l (Fig. A1a), with an increase in N leading to an increase in Chl$_l$ (for the same R$_{green}$), whereas Chl$_l$ will decrease if θ_l increases. The two-band enhanced vegetation index (EVI2, Jiang, Huete, Didan & Miura, 2008) is used as the primary LAI predictor, given its improved sensitivity over dense vegetation. In this study, EVI2 (Table A1) is used in place of the three-band EVI (Huete et al., 2002) due to difficulties matching observed and modeled reflectance values in the blue band. While the index normalization causes changes in N to have a relatively minor influence on simulated EVI2–LAI relationships, they remain strongly affected by variations in θ_l (Fig. A1b). At high vegetation densities, C_m also becomes a controlling factor (Fig. A1b). While normalized vegetation indices typically reduce the effect of confounding factors, single band reflectance relationships like LAI–R$_{nir}$ and Chl$_l$–R$_{green}$ (Table A1) maintain improved sensitivity over a wider range in LAI and Chl$_l$, respectively (Houborg, Anderson & Daughtry, 2009). In any case, proper determination of N, θ_l and C_m is critical for reliable estimation of Chl$_l$ and LAI when using Landsat-based spectral relationships as predictors.

Table A1

List of spectral bands and indices dedicated for Chl$_l$ and LAI retrieval as part of the REGFLEC iterative LUT approach (section A.3–A.6). LUTs are generated for each of these given the parameter ranges listed in Table A2. R_{nir} is near-infrared reflectance, R_{green} is the green band reflectance, NDVI is the normalized difference vegetation index, EVI2 is the two-band enhanced vegetation index, and MTVI2 is the second modified triangular vegetation index. The normalized difference vegetation index using red and green band reflectances (RGVI) is adopted here for predicting spatial variations in f$_B$ (section A.7).

Index	Formula	Reference
LAI = f(R$_{nir}$)	R_{nir}	
LAI = f(NDVI)	$(R_{nir} - R_{red})/(R_{nir} + R_{red})$	Rouse, Haas, Schell, & Deering (1974)
LAI = f(EVI2)	$2.5(R_{nir} - R_{red})/(R_{nir} + 2.4R_{red} - 1)$	Jiang, Huete, Didan and Miura (2008)
LAI = f(MTVI2)	$\dfrac{1.5\left[1.2\left(R_{nir}-R_{green}\right)-2.5\left(R_{red}-R_{green}\right)\right]}{\sqrt{(2R_{nir}+1)^2 - \left(6R_{nir}-5\sqrt{R_{red}}\right)-0.5}}$	Haboudane, Miller, Pattey, Zarco-Tejada, & Strachan (2004)
Chl = f(R$_{green}$)	R_{green}	
f$_B$ = f(RGVI)	$(R_{red} - R_{green})/(R_{red} + R_{green})$	

Table A2

Specific values and ranges for 8 input parameters used for building multi-dimensional LUTs of the spectral bands and indices listed in Table A1. For some parameters, the LUTs are only computed for a few entries but REGFLEC considers parameter values that fall in between the respective LUT entries by linearly interpolating between bounding parameter values (Houborg, Anderson & Daughtry, 2009).

Parameter	Abbr	Unit	LUT entries
Leaf area index	LAI	m^2 m^{-2}	0.2,0.7,1.2,1.7,2.2,2.7,3.2,3.7,4.2,4.7,5.2,5.7,6.2,6.7,7.2,7.7
Leaf chlorophyll content	Chl	μg cm^{-2}	14,20,26,32,38,44,50,56,62,68,74,80,86
Mean leaf inclination angle	θ$_l$	Deg	5,10,15,20,25,30,35,40,45,50,55,60,65,70,75,80,85
Leaf structure parameter	N		1.0,2.0,4.0
Dry matter content	C$_m$	g m^{-2}	10,200
Canopy fraction of senescent material	f$_B$		0.0,0.2,0.4,0.6,0.8
Soil parameter	s$_1$		0.1,0.25,0.6
Soil parameter	s$_2$		−0.1,0.0,0.1
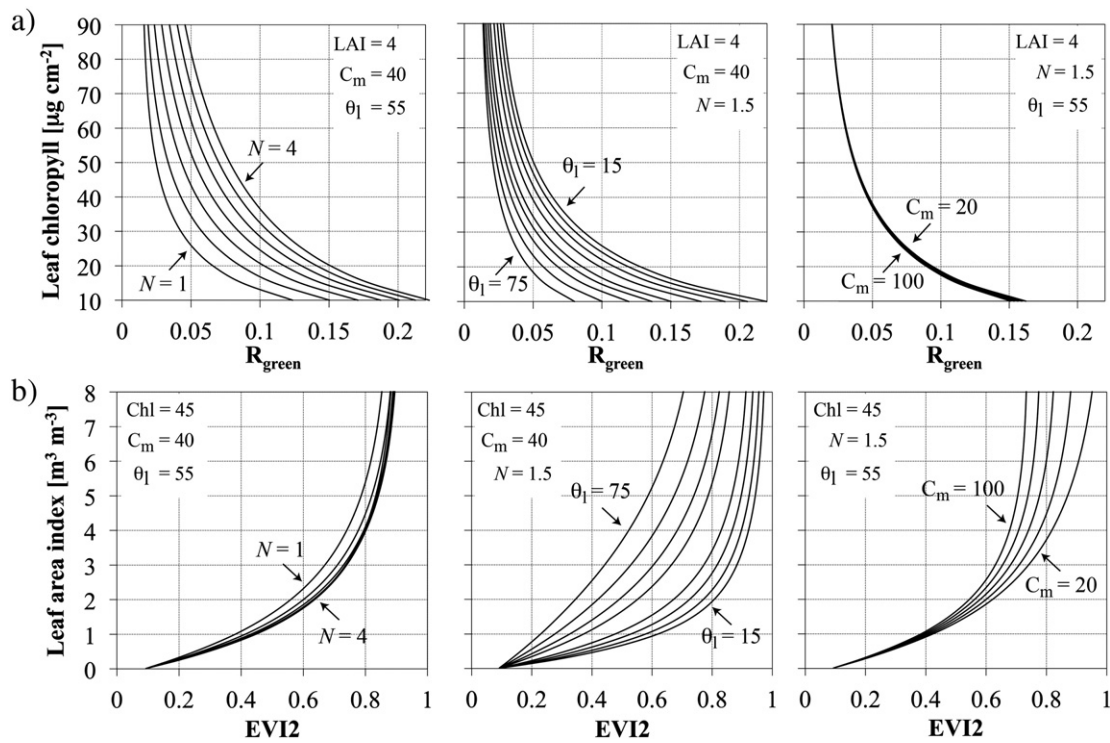
Fig. A1. Suite of predictive Chl$_l$–R$_{green}$ (a) and LAI–EVI2 (b) relationships established by running SAIL-PROSPECT with varying N, θ_l and C_m and LAI and Chl$_l$ fixed as indicated. In all runs, $\theta_s = 27$, $\theta_v = 1.5$, $s_1 = 0.2$ and $s_2 = 0$.

A.4. Initial soil background estimation (step 5)

The estimation of soil parameters (s$_1$ and s$_2$) is separated from the estimation of class-specific vegetation parameters (Section A.5) to minimize potentially confounding influences of the background reflectance signal on the Chl$_l$ and LAI retrievals. The basics behind the s$_1$ and s$_2$ retrieval and spatial extrapolation technique for sparsely vegetated pixels are described in detail in Houborg and Boegh (2008). To summarize, REGFLEC identifies bare soil or low vegetation pixels in the scene and estimates s$_1$ for each of these by iteratively changing s$_1$ and s$_2$ until the

MAE between satellite observed and modeled reflectances (R_{green}, R_{red} and R_{nir}) is minimized. The modeled reflectances are derived from LUTs accessed in inverse mode (Section A.3), assuming default vegetation parameter and Chl_l entry values (Houborg, Anderson & Daughtry, 2009) and using spatialized LAI estimates. The latter is calculated from a weighted combination of LUT-based LAI–NDVI relationships (Section A.3) with input of Landsat reflectance data. As the technique is only meaningful for low vegetation cover, derived LAI must be below 0.5 for s_1 and s_2 to be retrieved reliably. This condition is often difficult to meet, leading to large spatial gaps in the soil parameter maps. As a result, REGFLEC may initially be run for a scene with predominantly sparse vegetation coverage (preferably just before the growing season) in order to more effectively establish the spatial variability in the soil signal. The resulting s_1 and s_2 maps are then used to fill gaps in subsequent scenes with more vegetation coverage.

REGFLEC attempts to incorporate changes in soil brightness between the pre-growing season image and subsequent scenes. Since the second soil parameter, s_2, only accounts for approximately 20% of the spectral variability in the soil reflectance (Price, 1990), s_2 is assumed conservative in time and all brightness changes attributed to s_1 variations. A multivariate linear regression is established in order to relate s_1 in the active scene to the a priori (i.e. pre-growing season) s_1 and s_2 values. The regression is based on retrievals over pixels identified as soil (or sparsely vegetated) in both scenes and subsequently used to fill gaps at vegetated pixels with input of the bare soil (pre-growing season) s_1 and s_2 values. If available, an ancillary soil texture map may be used to extrapolate s_1 to unfilled vegetated pixels (LAI > 0.5) as described in Houborg and Anderson (2009). Otherwise, the extrapolation to unfilled pixels is based on land cover class and proximity to valid soil pixels. The resulting s_1 map provides a first estimate of the soil background signal. The reliability of the retrievals depends in part on the availability of sufficient a priori s_1 estimates and matching s_1 pairs to generate meaningful transfer functions and properly adjust for soil brightness changes between the two scenes. A pixel-wise refinement of s_1 is implemented in Section A.6 in an attempt to adjust for surface roughness and moisture variability not captured by the initial estimates.

A.5. Class-specific parameter retrievals (step 6)

In an attempt to constrain the inverse retrieval of LAI and Chl_l from the spectral reflectance signal, N, C_m and to some extent θ_l (see below), are assumed to remain constant within a given land cover class over the course of a growing season (Houborg & Anderson, 2009). A key new attribute of REGFLEC is the option to simultaneously exploit spectral observations (over intermediate to dense vegetation) from multiple satellite scenes over a growing season, which is typically available in the case of Landsat. The retrieval of optimal sets of class-invariant vegetation parameters relies on the availability of intermediate to dense vegetation pixels, where the contribution of the background signal to the overall scene reflectance is reduced and the total amount of radiation scatter by plants is increased (Daughtry, Walthall, Kim & Colstoun, 2000), which maximizes the sensitivity of the reflectance signal to variations in N, C_m and θ_l.

Initial class-specific pixel selection is based on a default NDVI threshold of 0.7. Further screening is performed to only include the most dense vegetation pixels at each acquisition time. At the same time, pixels on the boundary of land cover classes are omitted to avoid mixed pixels. Using an iterative LUT approach, REGFLEC then loops through all plausible parameter combinations of N (1.0, 1.2…4.0), θ_l (15, 20…80), and C_m (20, 40, 60, 80) and for each combination calculates initial LAI (as a function of observed R_{nir}) and Chl_l (as a function of observed R_{green}) for all selected class-specific pixels. With Chl_l calculated, LAI is updated as a function of EVI2. The relevant Chl and LAI relationships are established by accessing the appropriate scene-specific LUTs (Section A.3), using the initial estimates of soil parameters (Section A.4). These spatio-temporal Chl and LAI estimates are then input to the LUTs

for retrieving modeled spectral reflectances (R_{green}, R_{red}, R_{nir}) for each high NDVI pixel. The optimal class-specific parameter combination (i.e. N, θ_l, C_m) is the one that results in the smallest relative MAE between the multi-scene modeled and observed spectral reflectances, while assuring that Chl_l and LAI of associated pixels remain within a realistic range (Table A2).

Due to the ill-posed nature of model inversion (Combal, Baret, Weiss & Trubuil, 2002), different parameter settings may yield identical reflectance spectra. As such, it can be very difficult to separate relative contributions of LAI and Chl_l from the total reflectance signal (Wu, Niu, Tang & Huang, 2008). While the use of multi-scene spectral observations, as described above, represents a temporal regularization technique that can be helpful in guiding the inverse retrieval process, REGFLEC may also embed ancillary LAI, derived independently from satellite data (Section A.7), as a constraint on the parameter retrievals. The ancillary LAI is integrated into the routines described above to 1) select class-specific pixels suited for the inversion (LAI > 2), 2) estimate initial LAI (instead of LAI–R_{nir} relationships), and 3) calculate modeled spectral reflectances (a weighted average of REGFLEC and ancillary LAI is used).

Imposing temporal constraints on N and C_m is meaningful as they are typically fairly constant over the growing season for a given species type (Hosgood et al., 1995). θ_l may exhibit greater intra-class variability dependent on phenological stage (Huemmrich, 2013; Ross, 1981) and information on θ_l in space and time should ideally come from independent sources such as multi-angular satellite imagery. However, such information is currently not available. In REGFLEC, when ancillary LAI is used, spatio-temporal patterns in θ_l is deduced from LUT-based θ_l–R_{nir} relationships using input of ancillary LAI and iterated parameter combinations (N and C_m). This is a reasonable approximation as, for a given LAI, the near-infrared reflectance plateau is primarily modulated by θ_l (Asner, 1998). Following the class-specific parameter estimations, additional fine-tuning of θ_l is done independently for each scene by iteratively varying θ_l (class averaged value ± 15) over high vegetation density pixels to optimize the match between observed and modeled spectral reflectances. The resulting θ_l output is smoothed (to minimize intra-field variability) and extrapolated to all class-specific pixels based on proximity in space and time to a valid pixel retrieval.

A.6. LAI and Chl_l retrieval (step 7)

Following the class-specific multi-scene determination of N, θ_l, and C_m, each satellite scene is processed individually for estimating optimal Chl_l and LAI for all pixels within each land cover class, by iteratively adjusting s_1 and f_B (if applicable), as outlined in Houborg and Anderson (2009). Chl_l is mapped over the modeling domain using model-diagnosed Chl–R_{green} relationships, reflecting differences in LAI, land cover (N, θ_l, C_m), view-sun geometry, soil background (s_1, s_2) and degree of senescence (f_B, if applicable). A combination of LAI–MTVI2, LAI–EVI2 and LAI–R_{nir} relationships (Table A1) are used to derive the final LAI product. Ancillary LAI may be used as an additional constraint on the pixel-wise retrievals using the approach described in Section A.5. Note that adopted VI relationships are exclusively model derived and that no site-specific (in-situ) data are used for calibration purposes.

When REGFLEC is applied to multiple scenes, the activation of the f_B module (for considering leaf senescence) will be determined automatically for each class based on ancillary LAI or EVI2 time-series data (significant continuous declines in LAI/EVI2 are assumed indicative of senescence onset). During senescence, further increases in Chl_l and total LAI are assumed unlikely and predictions are constrained by penalizing combinations (s_1, f_B) that result in an increase in Chl_l or total LAI, or a decrease in f_B relative to the retrievals from the preceding Landsat scene at corresponding pixel locations. There is a strong link between f_B and the differences between red and green reflectances, as increasing the amount of senescent leaf material causes an increase in red relative to green reflectance (Houborg, Anderson & Daughtry, 2009). As a result, REGFLEC adopts f_B–RGVI relationships (Table A1) for the delineation of

horizontal f_B gradients. For any iterated f_B value, appropriate f_B–RGVI relationships (LUTs) are accessed and applied for disaggregating f_B onto each pixel. These are then used to update the green LAI and total (green + senescent) Chl_l values.

A.7. Ancillary LAI constraint

Some studies have shown increased robustness when integrating leaf level biochemical variables to the canopy level (e.g. leaf Chl × LAI) (Baret et al., 2007; Gitelson, Vina, Ciganda, Rundquist & Arkebauer, 2005; Weiss, Baret, Myneni, Pragnère & Knyazikhin, 2000) as leaf and canopy scale variables can have a mutually compensating effect on canopy reflectance (Lewis & Disney, 2007). Ancillary LAI may be used within the REGFLEC retrieval scheme (Section A.5 and A.6) in order to better separate LAI and Chl_l effects on observed reflectance spectra. Since other model parameters (N, θ_l, C_m) are kept free with wide ranges (Table A2), this LAI constraint could prove to be particularly important for regularization purposes. REGFLEC embeds an automated routine for retrieving ancillary LAI from Landsat using MODIS LAI products as reference (Gao, Anderson, Kustas & Wang, 2012). In this approach, homogeneous and high-quality LAI retrievals from MODIS (1 km) are used as references to develop a regression tree relating these MODIS LAI samples to atmospherically corrected Landsat surface reflectances derived using the Landsat ecosystem disturbance adaptive processing system (LEDAPS) (Masek et al., 2006). Landsat bands 2–5 and 7 are used to build the regression tree and multiple MODIS and Landsat image pairs are used in the process to include a wider range of sampled LAI. The same regression tree is then applied to all Landsat scenes for producing LAI values at 30 m resolution that are consistent with the MODIS LAI product. Evaluations against field measurements have shown that this approach can produce accurate estimates of LAI from Landsat (Gao, Anderson, Kustas & Wang, 2012).

Appendix B. Supplementary data

Supplementary data to this article can be found online at http://dx.doi.org/10.1016/j.rse.2014.12.008.

References

Asner, G.P. (1998). Biophysical and biochemical sources of variability in canopy reflectance. *Remote Sensing of Environment*, 64, 234–253. http://dx.doi.org/10.1016/S0034-4257(98)00014-5.

Atzberger, C. (2004). Object-based retrieval of biophysical canopy variables using artificial neural nets and radiative transfer models. *Remote Sensing of Environment*, 93, 53–67. http://dx.doi.org/10.1016/j.rse.2004.06.016.

Atzberger, C., & Richter, K. (2012). Spatially constrained inversion of radiative transfer models for improved LAI mapping from future Sentinel-2 imagery. *Remote Sensing of Environment*, 120, 208–218. http://dx.doi.org/10.1016/j.rse.2011.10.035.

Bacour, C., Baret, F., Béal, D., Weiss, M., & Pavageau, K. (2006). Neural network estimation of LAI, fAPAR, fCover and LAI × Cab, from top of canopy MERIS reflectance data: Principles and validation. *Remote Sensing of Environment*, 105, 313–325. http://dx.doi.org/10.1016/j.rse.2006.07.014.

Bacour, C., Jacquemoud, S., Leroy, M., Hautecœur, O., Weiss, M., Prévot, L., et al. (2002). Reliability of the estimation of vegetation characteristics by inversion of three canopy reflectance models on airborne POLDER data. *Agronomie, 22*, 555–565.

Baret, F. (1991). Vegetation canopy reflectance: Factors of variation and application for agriculture. In D. Hunt (Ed.), *Physical measurements and signatures in remote sensing* (pp. 145–167). France: Courchevel.

Baret, F., & Buis, S. (2008). Estimating canopy characteristics from remote sensing observations: Review of methods and associated problems. *Advances in land remote sensing: System, modeling, inversion and application* (pp. 173–201). Springer Verlag.

Baret, F., & Fourty, T. (1997). Estimation du contenu en eau et de la masse seche surfacique des feuilles a partir de spectres de reflectance et de transmittance. *Agronomie, 17*, 455–464.

Baret, F., Hagolle, O., Geiger, B., Bicheron, P., Miras, B., Huc, M., et al. (2007). LAI, fAPAR and fCover CYCLOPES global products derived from VEGETATION. *Remote Sensing of Environment*, 110, 275–286. http://dx.doi.org/10.1016/j.rse.2007.02.018.

Baret, F., Weiss, M., Lacaze, R., Camacho, F., Makhmara, H., Pacholcyzk, P., et al. (2013). GEOV1: LAI and FAPAR essential climate variables and FCOVER global time series capitalizing over existing products. Part1: Principles of development and production. *Remote Sensing of Environment*, 137, 299–309. http://dx.doi.org/10.1016/j.rse.2012.12.027.

Blackburn, G.A. (2007). Hyperspectral remote sensing of plant pigments. *Journal of Experimental Botany*, 58, 855–867. http://dx.doi.org/10.1093/jxb/erl123.

Bonan, G.B., Lawrence, P.J., Oleson, K.W., Levis, S., Jung, M., Reichstein, M., et al. (2011). Improving canopy processes in the Community Land Model version 4 (CLM4) using global flux fields empirically inferred from FLUXNET data. *Journal of Geophysical Research*, 116, 1–22. http://dx.doi.org/10.1029/2010JG001593.

Botha, E.J., Leblon, B., Zebarth, B., & Watmough, J. (2007). Non-destructive estimation of potato leaf chlorophyll from canopy hyperspectral reflectance using the inverted PROSAIL model. *International Journal of Applied Earth Observation and Geoinformation*, 9, 360–374. http://dx.doi.org/10.1016/j.jag.2006.11.003.

Botha, E.J., Leblon, B., Zebarth, B.J., & Watmough, J. (2010). Non-destructive estimation of wheat leaf chlorophyll content from hyperspectral measurements through analytical model inversion. *International Journal of Remote Sensing*, 31, 1679–1697. http://dx.doi.org/10.1080/01431160902926574.

Campbell, G.S. (1986). Extinction coefficients for radiation in plant canopies calculated using an ellipsoidal inclination angle distribution. *Agricultural and Forest Meteorology*, 36, 317–321.

Chen, J.M., & Cihlar, J. (1996). Retrieving leaf area index of boreal conifer forests using landsat TM images. *Remote Sensing of Environment*, 55, 153–162.

Ciganda, V., Gitelson, A., & Schepers, J. (2008). Vertical profile and temporal variation of chlorophyll in maize canopy: Quantitative "crop vigor" indicator by means of reflectance-based techniques. *Agronomy Journal*, 100, 1409–1417. http://dx.doi.org/10.2134/agronj2007.0322.

Ciganda, V., Gitelson, A., & Schepers, J. (2009). Non-destructive determination of maize leaf and canopy chlorophyll content. *Journal of Plant Physiology*, 166, 157–167. http://dx.doi.org/10.1016/j.jplph.2008.03.004.

Ciganda, V.S., Gitelson, A.A., & Schepers, J. (2012). How deep does a remote sensor sense? Expression of chlorophyll content in a maize canopy. *Remote Sensing of Environment*, 126, 240–247. http://dx.doi.org/10.1016/j.rse.2012.08.019.

Clevers, J.G.P.W., & Gitelson, A.A. (2013). Remote estimation of crop and grass chlorophyll and nitrogen content using red-edge bands on Sentinel-2 and -3. *International Journal of Applied Earth Observation and Geoinformation*, 23, 344–351. http://dx.doi.org/10.1016/j.jag.2012.10.008.

Clevers, J.G.P.W., & Kooistra, L. (2012). Using hyperspectral remote sensing data for retrieving canopy chlorophyll and nitrogen content. *IEEE Journal of Selected Topics in Applied Earth Observations and Remote Sensing*, 5, 574–583. http://dx.doi.org/10.1109/JSTARS.2011.2176468.

Comar, A., Baret, F., Obein, G., Simonot, L., Meneveaux, D., Viénot, F., et al. (2014). ACT: A leaf BRDF model taking into account the azimuthal anisotropy of monocotyledonous leaf surface. *Remote Sensing of Environment*, 143, 112–121. http://dx.doi.org/10.1016/j.rse.2013.12.006.

Combal, B., Baret, F., Weiss, M., & Trubuil, A. (2002). Retrieval of canopy biophysical variables from bidirectional reflectance: Using prior information to solve the ill-posed inverse problem. *Remote Sensing of Environment, 84*, 1–15.

Darvishzadeh, R., Skidmore, A., Schlerf, M., & Atzberger, C. (2008). Inversion of a radiative transfer model for estimating vegetation LAI and chlorophyll in a heterogeneous grassland. *Remote Sensing of Environment*, 112, 2592–2604. http://dx.doi.org/10.1016/j.rse.2007.12.003.

Dash, J., & Curran, P.J. (2007). Evaluation of the MERIS terrestrial chlorophyll index (MTCI). *Advances in Space Research*, 39, 100–104. http://dx.doi.org/10.1016/j.asr.2006.02.034.

Daughtry, C.S.T., Walthall, C.L., Kim, M.S., & Colstoun, E.B. De (2000). Estimating corn leaf chlorophyll concentration from leaf and canopy reflectance. *Remote Sensing of Environment*, 229–239.

Delegido, J., Alonso, L., González, G., & Moreno, J. (2010). Estimating chlorophyll content of crops from hyperspectral data using a normalized area over reflectance curve (NAOC). *International Journal of Applied Earth Observation and Geoinformation*, 12, 165–174. http://dx.doi.org/10.1016/j.jag.2010.02.003.

Delegido, J., Vergara, C., Verrelst, J., Gandía, S., & Moreno, J. (2011). Remote estimation of crop chlorophyll content by means of high-spectral-resolution reflectance techniques. *Agronomy Journal*, 103, 1834. http://dx.doi.org/10.2134/agronj2011.0101.

Demarez, V., Duthoit, S., Baret, F., Weiss, M., & Dedieu, G. (2008). Estimation of leaf area and clumping indexes of crops with hemispherical photographs. *Agricultural and Forest Meteorology*, 148, 644–655. http://dx.doi.org/10.1016/j.agrformet.2007.11.015.

Dorigo, W., Richter, R., Baret, F., Bamler, R., & Wagner, W. (2009). Enhanced automated canopy characterization from hyperspectral data by a novel two step radiative transfer model inversion approach. *Remote Sensing*, 1, 1139–1170. http://dx.doi.org/10.3390/rs1041139.

Dorigo, W.A., Zurita-Milla, R., de Wit, A.J.W., Brazile, J., Singh, R., & Schaepman, M.E. (2007). A review on reflective remote sensing and data assimilation techniques for enhanced agroecosystem modeling. *International Journal of Applied Earth Observation and Geoinformation*, 9, 165–193. http://dx.doi.org/10.1016/j.jag.2006.05.003.

Duthoit, S., Demarez, V., Gastellu-Etchegorry, J. -P., Martin, E., & Roujean, J. -L. (2008). Assessing the effects of the clumping phenomenon on BRDF of a maize crop based on 3D numerical scenes using DART model. *Agricultural and Forest Meteorology*, 148, 1341–1352. http://dx.doi.org/10.1016/j.agrformet.2008.03.011.

Ershadi, A., McCabe, M.F., Evans, J.P., Mariethoz, G., & Kavetski, D. (2013). A Bayesian analysis of sensible heat flux estimation: Quantifying uncertainty in meteorological forcing to improve model prediction. *Water Resources Research*, 49, 2343–2358. http://dx.doi.org/10.1002/wrcr.20231.

España, M., Baret, F., Chelle, M., Aries, F., & Andrieu, B. (1998). A dynamic model of maize 3D architecture: Application to the parameterisation of the clumpiness of the canopy. *Agronomie*, 18, 609–626.

Evans, J. (1989). Photosynthesis and nitrogen relationships in leaves of C3 plants. *Oecologia*, 78, 9–19.

Fensholt, R., Sandholt, I., & Stisen, S. (2006). Evaluating MODIS, MERIS, and VEGETATION vegetation indices using in situ measurements in a semiarid environment. *IEEE Transactions on Geoscience and Remote Sensing, 44,* 1774–1786. http://dx.doi.org/10.1109/TGRS.2006.875940.

Feret, J. -B., François, C., Asner, G.P., Gitelson, A.A., Martin, R.E., Bidel, L.P.R., et al. (2008). PROSPECT-4 and 5: Advances in the leaf optical properties model separating photosynthetic pigments. *Remote Sensing of Environment, 112,* 3030–3043. http://dx.doi.org/10.1016/j.rse.2008.02.012.

Feret, J. -B., François, C., Gitelson, A., Asner, G.P., Barry, K.M., Panigada, C., et al. (2011). Optimizing spectral indices and chemometric analysis of leaf chemical properties using radiative transfer modeling. *Remote Sensing of Environment, 115,* 2742–2750. http://dx.doi.org/10.1016/j.rse.2011.06.016.

Ganguly, S., Nemani, R.R., Zhang, G., Hashimoto, H., Milesi, C., Michaelis, A., et al. (2012). Generating global Leaf Area Index from Landsat: Algorithm formulation and demonstration. *Remote Sensing of Environment, 122,* 185–202. http://dx.doi.org/10.1016/j.rse.2011.10.032.

Gao, F., Anderson, M.C., Kustas, W.P., & Houborg, R. (2014). Retrieving Leaf Area Index from Landsat using MODIS LAI products and field measurements. *IEEE Geoscience and Remote Sensing Letters, 11,* 773–777. http://dx.doi.org/10.1109/LGRS.2013.2278782.

Gao, F., Anderson, M.C., Kustas, W.P., & Wang, Y. (2012). Simple method for retrieving leaf area index from Landsat using MODIS leaf area index products as reference. *Journal of Applied Remote Sensing, 6,* 63515–63554. http://dx.doi.org/10.1117/1.JRS.6.063554.

Gao, F., Masek, J., Schwaller, M., & Hall, F. (2006). On the blending of the Landsat and MODIS surface reflectance: predicting daily Landsat surface reflectance. *IEEE Transactions on Geoscience and Remote Sensing, 44,* 2207–2218. http://dx.doi.org/10.1109/TGRS.2006.872081.

Garrigues, S., Lacaze, R., Baret, F., Morisette, J.T., Weiss, M., Nickeson, J.E., et al. (2008). Validation and intercomparison of global Leaf Area Index products derived from remote sensing data. *Journal of Geophysical Research, 113.* http://dx.doi.org/10.1029/2007JG000635.

Gastellu-Etchegorry, J. (1996). Modeling radiative transfer in heterogeneous 3-D vegetation canopies. *Remote Sensing of Environment, 58,* 131–156. http://dx.doi.org/10.1016/0034-4257(95)00253-7.

Gitelson, A.A., Gritz, Y., & Merzlyak, M.N. (2003). Relationships between leaf chlorophyll content and spectral reflectance and algorithms for non-destructive chlorophyll assessment in higher plant leaves. *Journal of Plant Physiology, 160,* 271–282. http://dx.doi.org/10.1078/0176-1617-00887.

Gitelson, A.A., Keydan, G.P., & Merzlyak, M.N. (2006). Three-band model for noninvasive estimation of chlorophyll, carotenoids, and anthocyanin contents in higher plant leaves. *Geophysical Research Letters, 33,* L11402. http://dx.doi.org/10.1029/2006GL026457.

Gitelson, A.A., Peng, Y., Arkebauer, T.J., & Schepers, J. (2014). Relationships between gross primary production, green LAI, and canopy chlorophyll content in maize: Implications for remote sensing of primary production. *Remote Sensing of Environment, 144,* 65–72. http://dx.doi.org/10.1016/j.rse.2014.01.004.

Gitelson, A. a., Peng, Y., Masek, J.G., Rundquist, D.C., Verma, S., Suyker, A., et al. (2012). Remote estimation of crop gross primary production with Landsat data. *Remote Sensing of Environment, 121,* 404–414. http://dx.doi.org/10.1016/j.rse.2012.02.017.

Gitelson, A.A., Vina, A., Arkebauer, T.J., Rundquist, D.C., Keydan, G., & Leavitt, B. (2003). Remote estimation of leaf area index and green leaf biomass in maize canopies. *Geophysical Research Letters, 30,* 1248. http://dx.doi.org/10.1029/2002GL016450.

Gitelson, A.A., Vina, A., Ciganda, V., Rundquist, D.C., & Arkebauer, T.J. (2005). Remote estimation of canopy chlorophyll content in crops. *Geophysical Research Letters, 32,* L08403. http://dx.doi.org/10.1029/2005GL022688.

Gitelson, A.A., Wardlow, B.D., Keydan, G.P., & Leavitt, B. (2007). An evaluation of MODIS 250-m data for green LAI estimation in crops. *Geophysical Research Letters, 34,* L20403. http://dx.doi.org/10.1029/2007GL031620.

Gobron, N., Pinty, B., & Verstraete, M.M. (1997). Theoretical limits to the estimation of the leaf area index on the basis of visible and near-infrared remote sensing data. *IEEE Transactions on Geoscience and Remote Sensing, 35,* 1438–1445. http://dx.doi.org/10.1109/36.649798.

Gobron, N., Pinty, B., Verstraete, M.M., & Govaerts, Y. (1997). A semidiscrete model for the scattering of light by vegetation. *Journal of Geophysical Research, D: Atmospheres, 102,* 9431–9446.

Goel, N. (1988). Models of vegetation canopy reflectance and their use in estimation of biophysical parameters from reflectance data. *Remote Sensing Reviews, 4,* 1–212.

Gray, J., & Song, C. (2012). Mapping leaf area index using spatial, spectral, and temporal information from multiple sensors. *Remote Sensing of Environment, 119,* 173–183. http://dx.doi.org/10.1016/j.rse.2011.12.016.

Groenendijk, M., Dolman, a. J., van der Molen, M.K., Leuning, R., Arneth, a., Delpierre, N., et al. (2011). Assessing parameter variability in a photosynthesis model within and between plant functional types using global Fluxnet eddy covariance data. *Agricultural and Forest Meteorology, 151,* 22–38. http://dx.doi.org/10.1016/j.agrformet.2010.08.013.

Guindin-Garcia, N., Gitelson, A.A., Arkebauer, T.J., Shanahan, J., & Weiss, A. (2012). An evaluation of MODIS 8- and 16-day composite products for monitoring maize green leaf area index. *Agricultural and Forest Meteorology, 161,* 15–25. http://dx.doi.org/10.1016/j.agrformet.2012.03.012.

Haboudane, D., Miller, J. R., Pattey, E., Zarco-Tejada, P. J., & Strachan, I. B. (2004). Hyperspectral vegetation indices and novel algorithms forpredicting green LAI of crop canopies: Modeling and validation in the context of precision agriculture. *Remote Sensing of Environment, 90*(3), 337–352. http://dx.doi.org/10.1016/j.rse.2003.12.013.

Han, W., Yang, Z., Di, L., & Mueller, R. (2012). CropScape: A Web service based application for exploring and disseminating US conterminous geospatial cropland data products for decision support. *Computers and Electronics in Agriculture, 84,* 111–123. http://dx.doi.org/10.1016/j.compag.2012.03.005.

Holben, B., Eck, T., Slutsker, I., Tanre, D., Buis, J., Setzer, A., et al. (1998). AERONET – A federated instrument network and data archive for aerosol characterization. *Remote Sensing of Environment, 66,* 1–16.

Hosgood, B., Jacquemoud, S., Andreoli, G., Verdebout, J., Pedrini, G., & Schmuck, G. (1995). *Leaf Optical Properties Experiment 93 (LOPEX93).*

Houborg, R., & Anderson, M.C. (2009). Utility of an image-based canopy reflectance modeling tool for remote estimation of LAI and leaf chlorophyll content at regional scales. *Journal of Applied Remote Sensing, 3,* 033529. http://dx.doi.org/10.1117/1.3141522.

Houborg, R., Anderson, M., & Daughtry, C. (2009). Utility of an image-based canopy reflectance modeling tool for remote estimation of LAI and leaf chlorophyll content at the field scale. *Remote Sensing of Environment, 113,* 259–274. http://dx.doi.org/10.1016/j.rse.2008.09.014.

Houborg, R., & Boegh, E. (2008). Mapping leaf chlorophyll and leaf area index using inverse and forward canopy reflectance modeling and SPOT reflectance data. *Remote Sensing of Environment, 112,* 186–202. http://dx.doi.org/10.1016/j.rse.2007.04.012.

Houborg, R., Cescatti, A., Migliavacca, M., & Kustas, W.P. (2013). Agricultural and Forest Meteorology Satellite retrievals of leaf chlorophyll and photosynthetic capacity for improved modeling of GPP . *Agricultural and Forest Meteorology, 177,* 10–23. http://dx.doi.org/10.1016/j.agrformet.2013.04.006.

Houborg, R., Soegaard, H., & Boegh, E. (2007). Combining vegetation index and model inversion methods for the extraction of key vegetation biophysical parameters using Terra and Aqua MODIS reflectance data. *Remote Sensing of Environment, 106,* 39–58. http://dx.doi.org/10.1016/j.rse.2006.07.016.

Huemmrich, K.F. (2013). *Simulations of seasonal and latitudinal variations in leaf inclination angle distribution: Implications for remote sensing 2013, 93–101.*

Huete, A., Didan, K., Miura, T., Rodriguez, E.P., Gao, X., & Ferreira, L.G. (2002). Overview of the radiometric and biophysical performance of the MODIS vegetation indices. *Remote Sensing of Environment, 83,* 195–213.

Hunt, E.R., Daughtry, C.S.T., Eitel, J.U.H., & Long, D.S. (2011). Remote sensing leaf chlorophyll content using a visible band index. *Agronomy Journal, 103,* 1090–1099. http://dx.doi.org/10.2134/agronj2010.0395.

Jacquemoud, S., Bacour, C., Poilve, H., & Frangi, J. -P. (2000). Comparison of four radiative transfer models to simulate plant canopies reflectance direct and inverse mode. *Remote Sensing of Environment, 74,* 471–481. http://dx.doi.org/10.1016/S0034-4257(00)00139-5.

Jacquemoud, S., & Baret, F. (1990). PROSPECT: A model of leaf optical properties spectra. *Remote Sensing of Environment, 34,* 75–91. http://dx.doi.org/10.1016/0034-4257(90)90100-Z.

Jacquemoud, S., Baret, F., Andrieu, B., Danson, F.M., & Jaggard, K. (1995). Extraction of vegetation biophysical parameters by inversion of the PROSPECT + SAIL models on sugar beet canopy reflectance data. Application to TM and AVIRIS sensors. *Remote Sensing of Environment, 52,* 163–172. http://dx.doi.org/10.1016/0034-4257(95)00018-V.

Jacquemoud, S., Verhoef, W., Baret, F., Bacour, C., Zarco-Tejada, P.J., Asner, G.P., et al. (2009). PROSPECT + SAIL models: A review of use for vegetation characterization. *Remote Sensing of Environment, 113,* S56–S66. http://dx.doi.org/10.1016/j.rse.2008.01.026.

Jiang, Z., Huete, A., Didan, K., & Miura, T. (2008). Development of a two-band enhanced vegetation index without a blue band. *Remote Sensing of Environment, 112,* 3833–3845. http://dx.doi.org/10.1016/j.rse.2008.06.006.

Jung, M., Vetter, M., Herold, M., Churkina, G., Reichstein, M., Zaehle, S., et al. (2007). Uncertainties of modeling gross primary productivity over Europe: A systematic study on the effects of using different drivers and terrestrial biosphere models. *Global Biogeochemical Cycles, 21,* 1–12. http://dx.doi.org/10.1029/2006GB002915.

Kalfas, J.L., Xiao, X., Vanegas, D.X., Verma, S.B., & Suyker, A.E. (2011). Modeling gross primary production of irrigated and rain-fed maize using MODIS imagery and CO2 flux tower data. *Agricultural and Forest Meteorology, 151,* 1514–1528. http://dx.doi.org/10.1016/j.agrformet.2011.06.007.

Kalma, J.D., McVicar, T.R., & McCabe, M.F. (2008). Estimating land surface evaporation: A review of methods using remotely sensed surface temperature data. *Surveys in Geophysics, 29,* 421–469. http://dx.doi.org/10.1007/s10712-008-9037-z.

Kaminski, T., Knorr, W., Scholze, M., Gobron, N., Pinty, B., Giering, R., et al. (2012). Consistent assimilation of MERIS FAPAR and atmospheric CO_2 into a terrestrial vegetation model and interactive mission benefit analysis. *Biogeosciences, 9,* 3173–3184. http://dx.doi.org/10.5194/bg-9-3173-2012.

Kattge, J., Díaz, S., Lavorel, S., Prentice, I.C., Leadley, P., Bönisch, G., et al. (2011). TRY – a global database of plant traits. *Global Change Biology, 17,* 2905–2935. http://dx.doi.org/10.1111/j.1365-2486.2011.02451.x.

Kattge, J., Knorr, W., Raddatz, T., & Wirth, C. (2009). Quantifying photosynthetic capacity and its relationship to leaf nitrogen content for global-scale terrestrial biosphere models. *Global Change Biology, 15,* 976–991. http://dx.doi.org/10.1111/j.1365-2486.2008.01744.x.

Knorr, W., & Heimann, M. (2001). Uncertainties in global terrestrial biosphere modeling: 1. A comprehensive sensitivity analysis with a new photosynthesis and energy balance scheme. *Global Biogeochemical Cycles, 15,* 207–225. http://dx.doi.org/10.1029/1998GB001059.

Knyazikhin, Y., Martonchik, J.V., Myneni, R.B., Diner, D.J., & Running, S.W. (1998). Synergistic algorithm for estimating vegetation canopy leaf area index and fraction of absorbed photosynthetically active radiation from MODIS and MISR data. *Journal of Geophysical Research, D: Atmospheres, 103,* 32257–32275.

Koetz, B., Baret, F., Poilvé, H., & Hill, J. (2005). Use of coupled canopy structure dynamic and radiative transfer models to estimate biophysical canopy characteristics. *Remote Sensing of Environment, 95,* 115–124. http://dx.doi.org/10.1016/j.rse.2004.11.017.

Kotchenova, S.Y., Vermote, E.F., Matarrese, R., & Klemm, F.J. (2006). Validation of a vector version of the 6S radiative transfer code for atmospheric correction of satellite data. Part I: path radiance. *Applied Optics*, 45, 6762–6774.

Kuusk, A. (1991). The hot spot effect in the leaf canopy. *Digest – International Geoscience and Remote Sensing Symposium (IGARSS)* (pp. 1555–1557). Publ by IEEE.

Kuusk, A. (2001). A two-layer canopy reflectance model. *Journal of Quantitative Spectroscopy and Radiation Transfer*, 71, 1–9.

Lauvernet, C., Baret, F., Hascoët, L., Buis, S., & Le Dimet, F. -X. (2008). Multitemporal-patch ensemble inversion of coupled surface–atmosphere radiative transfer models for land surface characterization. *Remote Sensing of Environment*, 112, 851–861. http://dx.doi.org/10.1016/j.rse.2007.06.027.

Le Maire, G., François, C., & Dufrêne, E. (2004). Towards universal broad leaf chlorophyll indices using PROSPECT simulated database and hyperspectral reflectance measurements. *Remote Sensing of Environment*, 89, 1–28. http://dx.doi.org/10.1016/j.rse.2003.09.004.

Lewis, P., & Disney, M. (2007). Spectral invariants and scattering across multiple scales from within-leaf to canopy. *Remote Sensing of Environment*, 109, 196–206. http://dx.doi.org/10.1016/j.rse.2006.12.015.

López-Lozano, R., Baret, F., Chelle, M., Rochdi, N., & España, M. (2007). Sensitivity of gap fraction to maize architectural characteristics based on 4D model simulations. *Agricultural and Forest Meteorology*, 143, 217–229. http://dx.doi.org/10.1016/j.agrformet.2006.12.005.

Malenovský, Z., Homolová, L., Zurita-Milla, R., Lukeš, P., Kaplan, V., Hanuš, J., et al. (2013). Retrieval of spruce leaf chlorophyll content from airborne image data using continuum removal and radiative transfer. *Remote Sensing of Environment*, 131, 85–102. http://dx.doi.org/10.1016/j.rse.2012.12.015.

Masek, J.G., Vermote, E.F., Saleous, N.E., Wolfe, R., Hall, F.G., Huemmrich, K.F., et al. (2006). A Landsat surface reflectance dataset. *Terra*, 3, 68–72.

Maxwell, S.K., Schmidt, G.L., & Storey, J.C. (2007). A multi-scale segmentation approach to filling gaps in Landsat ETM+ SLC-off images. *International Journal of Remote Sensing*, 28, 5339–5356. http://dx.doi.org/10.1080/01431160601034902.

McCabe, M.F., Kalma, J.D., & Franks, S.W. (2005). Spatial and temporal patterns of land surface fluxes from remotely sensed surface temperatures within an uncertainty modelling framework. *Hydrology and Earth System Sciences*, 9, 467–480.

Medvigy, D., Wofsy, S.C., Munger, J.W., Hollinger, D.Y., & Moorcroft, P.R. (2009). Mechanistic scaling of ecosystem function and dynamics in space and time: Ecosystem Demography model version 2. *Journal of Geophysical Research*, 114, G01002. http://dx.doi.org/10.1029/2008JG000812.

Myneni, R., Hoffman, S., Knyazikhin, Y., Privette, J., Glassy, J., Tian, Y., et al. (2002). Global products of vegetation leaf area and fraction absorbed PAR from year one of MODIS data. *Remote Sensing of Environment*, 83, 214–231. http://dx.doi.org/10.1016/S0034-4257(02)00074-3.

Pinty, B., Jung, M., Kaminski, T., Lavergne, T., Mund, M., Plummer, S., et al. (2011). Evaluation of the JRC-TIP 0.01° products over a mid-latitude deciduous forest site. *Remote Sensing of Environment*, 115, 3567–3581. http://dx.doi.org/10.1016/j.rse.2011.08.018.

Pisek, J., Ryu, Y., Sprintsin, M., He, L., Oliphant, A.J., Korhonen, L., et al. (2013). Retrieving vegetation clumping index from Multi-angle Imaging SpectroRadiometer (MISR) data at 275 m resolution. *Remote Sensing of Environment*, 138, 126–133. http://dx.doi.org/10.1016/j.rse.2013.07.014.

Price, J.C. (1990). On the information content of soil reflectance spectra. *Remote Sensing of Environment*, 33, 113–121.

Proud, S. R., Rasmussen, M. O., Fensholt, R., Sandholt, I., Shisanya, C., Mutero, W., et al. (2010). Improving the SMAC atmospheric correction code by analysis of Meteosat Second Generation NDVI and surface reflectance data. *Remote Sensing of Environment*, 114(8), 1687–1698. http://dx.doi.org/10.1016/j.rse.2010.02.020.

Richter, K., Atzberger, C., Vuolo, F., Weihs, P., & D'Urso, G. (2009). Experimental assessment of the Sentinel-2 band setting for RTM-based LAI retrieval of sugar beet and maize. *Canadian Journal of Remote Sensing*, 35, 230–247.

Rivera, J., Verrelst, J., Leonenko, G., & Moreno, J. (2013). Multiple cost functions and regularization options for improved retrieval of leaf chlorophyll content and LAI through inversion of the PROSAIL model. *Remote Sensing*, 5, 3280–3304. http://dx.doi.org/10.3390/rs5073280.

Ross, J. (1981). *The radiation regime and architecture of plant stands.* Springer. http://dx.doi.org/10.1007/978-94-009-8647-3.

Rouse, J. W., Haas, R.H., Schell, J.A., & Deering, D. W. (1974). *Monitoring vegetation systems in the Great Plains with ERTS, Third ERTS Symposium.* NASA SP-351 I, 309–317.

Sage, R.F., Pearcy, R.W., & Seeman, J.R. (1987). The nitrogen Use efficiency of C3 and C4 plants. *Plant Physiology*, 85, 355–359.

Schlemmer, M., Gitelson, A., Schepers, J., Ferguson, R., Peng, Y., Shanahan, J., et al. (2013). Remote estimation of nitrogen and chlorophyll contents in maize at leaf and canopy levels. *International Journal of Applied Earth Observation and Geoinformation*, 25, 47–54. http://dx.doi.org/10.1016/j.jag.2013.04.003.

Schlerf, M., & Atzberger, C. (2006). Inversion of a forest reflectance model to estimate structural canopy variables from hyperspectral remote sensing data. *Remote Sensing of Environment*, 100, 281–294. http://dx.doi.org/10.1016/j.rse.2005.10.006.

Sellers, P., Randall, D., Collatz, G., Berry, J., Field, C., Dazlich, D., et al. (1996). A revised land surface parameterization (SiB2) for atmospheric GCMs. Part I: Model Formulation. *Journal of Climate*, 9, 676–705.

Sims, D.A., & Gamon, J.A. (2002). Relationships between leaf pigment content and spectral reflectance across a wide range of species, leaf structures and developmental stages. *Remote Sensing of Environment*, 81, 337–354. http://dx.doi.org/10.1016/S0034-4257(02)00010-X.

Singh, S.K., Hoyos-Villegas, V., Ray, J.D., Smith, J.R., & Fritschi, F.B. (2013). Quantification of leaf pigments in soybean (Glycine max (L) Merr.) based on wavelet decomposition of hyperspectral features. *Field Crops Research*, 149, 20–32. http://dx.doi.org/10.1016/j.fcr.2013.04.019.

Tou, J. T., & Gonzalez, R. C. (1974). *Pattern recognition principles.* Massachusetts: Addison-Wesley, Reading.

Vanderbilt, V.C., Grant, L., & Daughtry, C.S.T. (1985). Polarization of light scattered by vegetation. *Proceedings of the IEEE*, 73, 1012–1024. http://dx.doi.org/10.1109/PROC.1985.13232.

Verhoef, W. (1984). Light scattering by leaf layers with application to canopy reflectance modeling: The SAIL model. *Remote Sensing of Environment*, 16, 125–141.

Verhoef, W. (1985). Earth observation modeling based on layer scattering matrices. *Remote Sensing of Environment*, 17, 165–178.

Verhoef, W., & Bach, H. (2003). Simulation of hyperspectral and directional radiance images using coupled biophysical and atmospheric radiative transfer models. *Remote Sensing of Environment*, 87(1), 23–41. http://dx.doi.org/10.1016/S0034-4257(03)00143-3.

Verhoef, W., & Bach, H. (2007). Coupled soil–leaf-canopy and atmosphere radiative transfer modeling to simulate hyperspectral multi-angular surface reflectance and TOA radiance data. *Remote Sensing of Environment*, 109, 166–182. http://dx.doi.org/10.1016/j.rse.2006.12.013.

Verhoef, W., Jia, L., Xiao, Q., & Su, Z. (2007). Unified optical-thermal four-stream radiative transfer theory for homogeneous vegetation canopies. *IEEE Transactions on Geoscience and Remote Sensing*, 45, 1808–1822. http://dx.doi.org/10.1109/TGRS.2007.895844.

Verma, S.B., Dobermann, A., Cassman, K.G., Walters, D.T., Knops, J.M., Arkebauer, T.J., et al. (2005). Annual carbon dioxide exchange in irrigated and rainfed maize-based agroecosystems. *Agricultural and Forest Meteorology*, 131, 77–96. http://dx.doi.org/10.1016/j.agrformet.2005.05.003.

Vermote, E.F., Tanre, D., Deuze, J.L., Herman, M., & Morcette, J. -J. (1997). Second simulation of the satellite signal in the solar spectrum, 6S: An overview. *IEEE Transactions on Geoscience and Remote Sensing*, 35, 675–686. http://dx.doi.org/10.1109/36.581987.

Viña, A., Gitelson, A.A., Nguy-Robertson, A.L., & Peng, Y. (2011). Comparison of different vegetation indices for the remote assessment of green leaf area index of crops. *Remote Sensing of Environment*, 115, 3468–3478. http://dx.doi.org/10.1016/j.rse.2011.08.010.

Vuolo, F., Dini, L., & D'Urso, G. (2008). Retrieval of Leaf Area Index from CHRIS/PROBA data: an analysis of the directional and spectral information content. *International Journal of Remote Sensing*, 29, 5063–5072. http://dx.doi.org/10.1080/01431160802036490.

Wang, Y.P., Baldocchi, D., Leuning, R., Falge, E., & Vesala, T. (2007). Estimating parameters in a land-surface model by applying nonlinear inversion to eddy covariance flux measurements from eight FLUXNET sites. *Global Change Biology*, 13, 652–670. http://dx.doi.org/10.1111/j.1365-2486.2006.01225.x.

Wang, Q., Tenhunen, J., Dinh, N., Reichstein, M., Otieno, D., Granier, A., et al. (2005). Evaluation of seasonal variation of MODIS derived leaf area index at two European deciduous broadleaf forest sites. *Remote Sensing of Environment*, 96, 475–484. http://dx.doi.org/10.1016/j.rse.2005.04.003.

Weiss, M., Baret, F., Myneni, R.B., Pragnère, A., & Knyazikhin, Y. (2000). Investigation of a model inversion technique to estimate canopy biophysical variables from spectral and directional reflectance data. *Agronomie*, 20, 3–22.

Wu, C., Niu, Z., Tang, Q., & Huang, W. (2008). Estimating chlorophyll content from hyperspectral vegetation indices: Modeling and validation. *Agricultural and Forest Meteorology*, 148, 1230–1241. http://dx.doi.org/10.1016/j.agrformet.2008.03.005.

Xu, L., & Baldocchi, D.D. (2003). Seasonal trends in photosynthetic parameters and stomatal conductance of blue oak (Quercus douglasii) under prolonged summer drought and high temperature. *Tree Physiology*, 23, 865–877.

Yang, W., Shabanov, N.V., Huang, D., Wang, W., Dickinson, R.E., Nemani, R.R., et al. (2006). Analysis of leaf area index products from combination of MODIS Terra and Aqua data. *Remote Sensing of Environment*, 104, 297–312. http://dx.doi.org/10.1016/j.rse.2006.04.016.

Zaehle, S. (2005). Effects of parameter uncertainties on the modeling of terrestrial biosphere dynamics. *Global Biogeochemical Cycles*, 19. http://dx.doi.org/10.1029/2004GB002395.

Zhu, Z., & Woodcock, C.E. (2012). Object-based cloud and cloud shadow detection in Landsat imagery. *Remote Sensing of Environment*, 118, 83–94. http://dx.doi.org/10.1016/j.rse.2011.10.028.